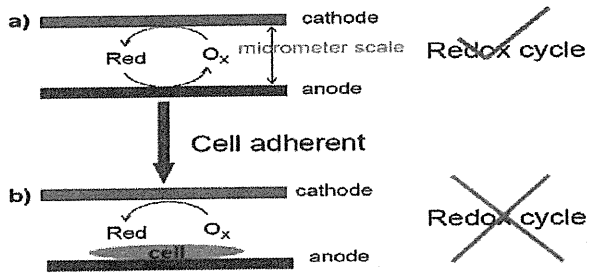

Fig. 3 The principle for cell topography detection. (a) Before cell adhesion; (b) after cell adhesion.

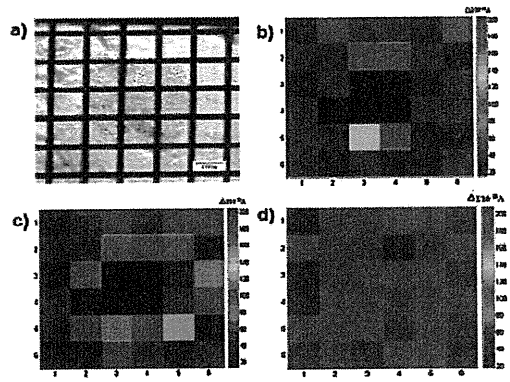

Fig. 4 (a) The image of cell topography obtained by microscopy, (b) the corresponding current image, (c) the current image after 24 h of additional cultivation, and (d) after treating with 2% methanol.

were kept open. For curve b, all column electrodes (C1–C6) had the same potential applied simultaneously, but only the current at C2 was read out. Both curves show a sigmoidal shape. In addition, the two curves show nearly identical behavior. This feature implies that the individual diffusion layers from the adjacent column electrodes did not overlap and, therefore, there was no interference from cross-talk between the column electrodes during the detection period.

The principle of cell topography imaging is shown in Fig. 3. If the redox compound showing reversible electrochemical behavior is present in the interspaces between the column and row electrodes set at appropriate potentials, the reduction and oxidation of the compound proceeds at the addressing point. This redox cycling, proceeding only at the designated addressing point, amplifies the electrochemical signal[16,17] (Fig. 3(a)). Since the magnitude of the amplified current has a direct relationship with the area of the electrode,[18] the current response or amplification efficiency becomes lower when the electrode at the addressing points is covered with insulating material, such as living cells. Therefore, the redox cycling will be blocked and the current amplification will be reduced (Fig. 3(b)) if cells grow adherently on the electrode surface at an addressing point. By sequentially changing the potential applied to different column and row electrodes and the read-out column electrode, as described in the experimental section, the current responses at each addressing point can be obtained to draw two-dimensional electrochemical responses, which in turn indicates the topography of the cells.

In our earlier study, a 4-aminophenol (PAP) and *p*-quinoneimine redox cycling system was used to study gene expression ability in single cells,[17] since PAP is a cellular membrane-permeable substance. To obtain a clear image based on the blockage of redox cycling, it is desirable to use a non-permeable redox species; thus, $K_3[Fe(CN)_6]$ was chosen as the species in this study, since $Fe(CN)_6^{3-}$ is non-permeable through the cell membrane.

In order to monitor cell topography and proliferation, it is necessary that the cells remain viable after detection. Cell viability was checked using Calcein-AM (Wako Pure Chemical Industries, Tokyo, Japan) and it was confirmed that all of the cells were alive for at least 30 min in the detection medium. Since the electrochemical detection in the medium was completed within 10 min, there should have been no significant influence on the viability during the electrochemical detection.

Before cell adhesion, the current amplification at each addressing point was investigated. The RSD (relative standard deviation) of the current amplification at the addressing points was 2.87%, indicating that all of the addressing points were under electrochemically equivalent circumstances. When the cell suspension in the detection medium with 4.0 mM $Fe(CN)_6^{3-}$ was introduced into the chip, the current responses or amplification efficiencies were found to be similar to those without the cells. This result indicates that the floating cells did not block the redox cycling of the $Fe(CN)_6^{3-}/Fe(CN)_6^{4-}$ redox couple at the addressing points.

Next, the electrochemical imaging of the cells on the substrate was investigated using the addressable device. Fig. 4 shows the optical photograph of the patterned cells and the electrochemical images observed with the addressable device. The area with low electrochemical responses (Fig. 4(b)) corresponds well with that of the topography of the patterned cells in the optical photograph (Fig. 4(a)), since the cells blocked the redox cycling of $Fe(CN)_6^{3-}/Fe(CN)_6^{4-}$. After the measurement, the device was disassembled and the cells were cultured for 24 h. The electrochemical image after the cultivation shows that the topography with low currents expanded (Fig. 4(c)) compared to the image in Fig. 4(b). During the cultivation, the HeLa cells proliferated and expanded the topography of the cell pattern on the substrate, causing partial coverage of the surrounding crossing points. This coverage decreased the amplification efficiency by redox cycling and lowered the current responses at the crossing points. With further cell culture, the area with low current responses became larger.

An *in vitro* cytotoxicity assay was considered as a promising alternative method to animal testing and has been applied to determine basic cytotoxicity and cell viability assessment. In the assay, the key issue was how to assess the numbers of viable and non-viable cells after exposure to special chemicals.[19] In the present study, we applied the proposed addressable device for cytotoxicity detection. Methanol was chosen as a toxic chemical for the model case. It is known that a solution containing 2% methanol is fatal to cells. After a clear topography of the patterned cells was observed (Fig. 4(c)), the solution inside the addressable device was changed to 4.0 mM $K_3[Fe(CN)_6]$ containing 2% methanol. The electrochemical responses at the topography area

increased gradually and reached a constant in 5 min. After 5 min, no topography was found in the electrochemical image (Fig. 4(d)). The methanol in the solution caused fatal damage to the cells, which detached from the substrate, thus leading to a recovery in redox cycling and current amplification at the crossing points. Thus, the topography of the cell pattern faded out from the electrochemical image on exposure to 2% methanol. These results indicate that the present electrochemical device is applicable for the investigation of cytotoxicity of various species.

The present study demonstrated an electrochemical method for detecting cell topography using an addressable electrochemical device with orthogonally arranged row/column electrode arrays. The presence of adherent cells at the addressing points blocks redox cycling between the row and column electrodes because the redox species do not permeate through the cell membrane. This blockage reduces the current response based on redox amplification. Since the current response depends on the status of the cells, concentration, proliferation of the adherent cells, and cytotoxicity effects can be monitored or imaged with the device. The present device can be applied to cell culture toxicology tests. Although in the present device, there is a problem with the changing of the solution, integration with a solution-changing system could facilitate the replacement of the solution in the gap regions between the row and column electrodes to make the device easier to handle when applying it to cytotoxicity studies. Further work in this direction is underway at our laboratory.

This study was supported by Special Coordination Funds for Promoting Science and Technology, Formation of Innovation Center for Fusion of Advanced Technologies, from Japan Science and Technology Agency, and by a Grant-in-Aid (445) for Science Research on Priority Areas "Life Surveyor" from MEXT, Japan. Z.Y also thanks the support of the National Basic Research Program of China (No. 2010CB732403), the NSFC (20735002,20905013), and the Special Foundation for Young Scientists of Fujian Province, China (2008F3057).

Notes and references

1 J. H. Yeon and J.-K. Park, *Anal. Biochem.*, 2005, **341**, 308.
2 R. E. White, *Annu. Rev. Pharmacol. Toxicol.*, 2000, **40**, 133.
3 B. Henderson, R. K. Ross and M. C. Pike, *Science*, 1991, **254**, 1131.
4 I. Giaever and C. R. Keese, *Proc. Natl. Acad. Sci. U. S. A.*, 1984, **81**, 3761.
5 I. Giaever and C. R. Keese, *Nature*, 1993, **366**, 591.
6 Y. L. Qiu, R. L. Liao and X. Zhang, *Anal. Chem.*, 2008, **80**, 990.
7 A. Chatterjee, C. Snead, G. Yetik-Anacak, G. Antonova, J. M. Zeng and J. D. Catravas, *Am. J. Physiol.: Lung Cell. Mol. Phys.*, 2008, **294**, L755.
8 C. Xiao and J. H. T. Luong, *Biotechnol. Prog.*, 2003, **19**, 1000.
9 L. Ceriotti, J. Ponti, F. Broggi, A. Kob, S. Drechsler, E. Thedinga, P. Colpo, E. Sabbioni, R. Ehret and F. Rossi, *Sens. Actuators, B*, 2007, **123**, 769.
10 N. C. Yu, J. M. Atienza, J. Bernard, S. Blanc, J. Zhu, X. B. Wang, X. Xu and Y. A. Abassi, *Anal. Chem.*, 2006, **78**, 35.
11 K. T. C. Chai, J. H. Daview and D. R. S. Cumming, *Sens. Actuators, B*, 2007, **127**, 97.
12 E. E. Krommenhoek, J. G. E. Gardeniers and J. G. Bomer, *Anal. Chem.*, 2007, **79**, 5567.
13 R. Ehret, W. Baumann, M. Brischwein, A. Schwinde, K. Stegbauer and B. Wolf, *Biosens. Bioelectron.*, 1997, **12**, 29.
14 L. Pitta Bauermann, W. Schuhmann and A. Schulte, *Phys. Chem. Chem. Phys.*, 2004, **6**, 4003.
15 C. Modin, L. Stranne, M. Foss, M. Duch, J. Justesen, J. Chevallier, L. K. Andersen, A. G. Hemmersam, F. S. Pedersen and F. Besenbacher, *Biomaterials*, 2006, **27**, 1346.
16 Z. Y. Lin, Y. Takahashi, Y. Kitagawa, T. Umemura, H. Shiku and T. Matsue, *Anal. Chem.*, 2008, **80**, 6830.
17 Z. Y. Lin, Y. Takahashi; T. Murata, M. Takeda, K. Ino, H. Shiku and T. Matsue, *Angew. Chem., Int. Ed.*, 2009, **48**, 2044.
18 T. Matsue, A. Aoki, T. Abe and I. Uchida, *Chem. Lett.*, 1989, 133.
19 F. Zucco, I. De Angelis, E. Testai and A. Stammati, *Toxicol. in Vitro*, 2004, **18**, 153.

Addressable electrochemiluminescence detection system based on redox-cycling of $Ru(bpy)_3^{2+}$ †

Zhenyu Lin,[a] Kosuke Ino,[b] Hitoshi Shiku,[b] Tomokazu Matsue*[b] and Guonan Chen*[a]

Received (in Cambridge, UK) 4th August 2009, Accepted 22nd October 2009
First published as an Advance Article on the web 16th November 2009
DOI: 10.1039/b915871e

This is the first report on addressable electrochemiluminescence (ECL) based on redox-cycling of tris(2,2′-bipyridine)-ruthenium(II) ($Ru(bpy)_3^{2+}$). By changing the column or row electrodes addressed, the ECL at each address point can be detected separately.

Electrochemiluminescence (ECL) is a chemiluminescent reaction of species generated electrochemically at an electrode surface, which is a sensitive and selective detection method having important applications in bioanalytical science. The ECL of tris(2,2′-bipyridine)-ruthenium(II) ($Ru(bpy)_3^{2+}$) was one of the mostly studied ECL systems since its first publication in 1966.[1–4] Different mechanisms can lead to the ECL of $Ru(bpy)_3^{2+}$, such as coreactant and annihilation ECL systems.[5] In the latter system, $Ru(bpy)_3^{2+}$ can be oxidized and reduced on a single electrode with high frequency to produce $Ru(bpy)_3^{3+}$ and $Ru(bpy)_3^{+}$, respectively, then the annihilation reaction between these two productions occurs to produce the excited $[Ru(bpy)_3^{2+}]^*$ and further to give ECL.[6] $Ru(bpy)_3^{2+}$ showed the character of redox-cycling during ECL reactions, the amount of $Ru(bpy)_3^{2+}$ had not been reduced. It is also possible to obtain emission at two different electrodes that are close enough to allow the electrogenerated reactants to interdiffuse and undergo annihilation.[7] For example, a rotating ring disk electrode can be applied to generate one reactant at the central disk while the other one is generated at the ring, then these two reactants diffuse and react to produce ECL.[8] Murry *et al.* studied the ECL of $Ru(bpy)_3^{2+}$ on micrometer-spaced platinum interdigitated electrodes.[9] Annihilation ECL with microelectrodes has been used to study sol–gel composites containing $Ru(bpy)_3^{2+}$ and diode-like chemiluminescence in frozen concentration gradients of the polymer poly-$[Ru(vbpy)_3](PF_6)_2$.[10] Hayase *et al.* used transparent conductive glass as two working electrodes, which were arranged face to face, with a gap left between the electrodes, it showed that high ECL intensity could be detected if the $Ru(bpy)_3(PF_6)_2$ being injected into the gap and the two electrodes had been set at an appropriate potential.[11] Michel *et al.* reported that protein–ruthenium chelate complexes could lead to redox-cycling type ECL in aqueous medium.[12] Based on this result, it is possible to develop the immunoassays involving redox-cycling type ECL as the detection principle. These studies showed it is easy to control the ECL by dual-working electrode systems and can lead to real applications.

In order to realize rapid, comprehensive and high-throughput analyses, there has been strong demand to develop array-based biosensors. Many array-based biosensors developed so far are based on fluorescence detection since fluorescence measurement usually has a high sensitivity. Another form of detection utilized in array-based biosensors is amperometric detection, which offers sufficient sensitivity as well as specificity. ECL detection has also been applied in array-based sensors. For example, Sojic *et al.* had developed an ordered array of optoelectrochemical, individually readable sensors which had an application in remote ECL imaging.[13] The sensors of the array can not be individually addressable electrochemically detected, but each addressable point is optically independent and individually readable.

In an early study, we put forward a novel electrochemical image system, which consisted of orthogonally arranged row/column electrode arrays, which have the benefits of easy fabrication and high integration.[14,15] Based on the redox-cycling of some electroactive compounds at the crossing points of the row/column electrodes, electrochemical response at each addressing point can be detected separately. In this research, detection of the $Ru(bpy)_3^{2+}$ ECL system has been coupled to the proposed device and a simple ECL image system has been developed. The two microelectrodes at the crossing points can be deemed as the dual-working electrode in the annihilation ECL reaction of $Ru(bpy)_3^{2+}$. Changing the addressing of the column and row electrodes, the crossing point will be changed too. In this way, the ECL at each crossing point can be detected separately or simultaneously.

Fig. 1(A,B) shows the scheme of the addressable micro-electrode array. Two platinum microbands (width: 50 μm; gab between the two microbands: 250 μm) were constructed on a glass substrate by using a photolithographic method.[14,15] Two holes were then made on one substrate by a CO_2 laser (M class, Universal Laser Systems, AZ, USA), the holes will serve as the inlet and the outlet for the ECL solution. The Su-8 sheet (15-μm thick; Nippon Kayaku Co. Ltd. Japan) was cut to required specifications and then two glass substrates with the microelectrode array were orthogonally glued face to face through the Su-8 sheet using a hard-bake (180 °C), and formed 4 orthogonal crossing points. The gap between the two substrates can contain solutions and act as a reaction well. The scheme of the ECL detection system was shown in Fig. 1(C), the detail of which is shown in the ESI.†

Fig. 2 highlights the principle of the row/column array architecture addressable ECL detection. During testing, the

[a] *The Key Lab of Analysis and Detection Technology for Food Safety of the MOE, Department of Chemistry, Fuzhou University, Fuzhou, 350002, China. E-mail: gnchen@fzu.edu.cn*
[b] *Graduate School of Environmental Studies, Tohoku University, 6-6-11 Aoba, Aramaki, Sendai 980-8579, Japan. E-mail: matsue@bioinfo.che.tohoku.ac.jp; Fax: (+86)591-83713866*
† Electronic supplementary information (ESI) available: Experimental details. See DOI: 10.1039/b915871e

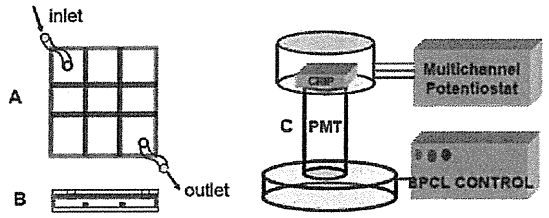

Fig. 1 Scheme of the addressable chip and the ECL detection chip. (A): top view of the chip; (B): side view of the chip; (C): scheme of the ECL detection system.

column and the row electrodes at the addressing points have been applied with appropriate potentials, one with oxidation potential and the other at the reduction potential, while all the other working electrodes were left open. When oxidation potential was applied to the addressed column electrode, $Ru(bpy)_3^{2+}$ could be oxidized to $Ru(bpy)_3^{3+}$, while $Ru(bpy)_3^{+}$ would be produced at the addressed row electrode, where a reduction potential had been applied. Then $Ru(bpy)_3^{3+}$ and $Ru(bpy)_3^{+}$ would diffuse from the electrode to the main solutions to react to produce the excited $[Ru(bpy)_3^{2+}]^*$. When $[Ru(bpy)_3^{2+}]^*$ goes back to its basic state, it produces ECL signals. From this mechanism, we know that in one reaction circle, the luminescent reagent has not been consumed, which shows the character of redox-cycling.

Of the other points on the chosen column or row electrodes, only $Ru(bpy)_3^{3+}$ or $Ru(bpy)_3^{+}$ has been produced, which cannot generate an ECL signal. While on the other electrodes that have not been addressed, no reaction happened. In this case, the ECL signals just come from the addressed points. By sequentially changing the potential applied to the column and row electrodes, we collected the ECL responses at the entire crossing point, allowing the system to be addressable. We can address different electrodes at the same time, in this case, we can detect the total ECL intensity from many addressing points.

The cyclic voltammogram of 1 mM $Ru(bpy)_3^{2+}$ had been examined, and it was found that on the anodic side, a clear peak could be observed at 1.2 V *versus* Pt, which was attributed to the redox cycle of $Ru(bpy)_3^{2+}/Ru(bpy)_3^{3+}$. On the cathodic side, another peak corresponding to the redox cycle of $Ru(bpy)_3^{2+}/Ru(bpy)_3^{+}$ appeared at −1.3 V. So in this study, 1.2 and −1.3 V were chosen. Fig. 3 shows the current and ECL recorded on one addressable point. From Fig. 3,

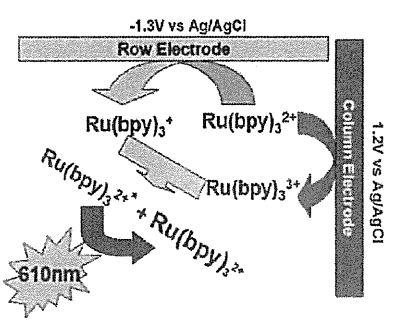

Fig. 2 Principle of the ECL reaction based on redox-cycling.

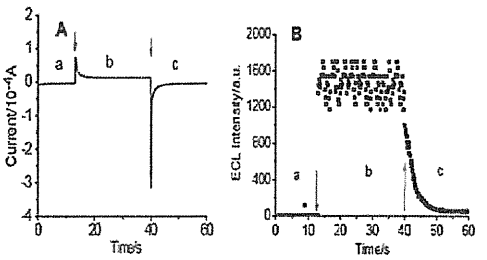

Fig. 3 Current recorded for one column electrode at a single addressing point (A) and the corresponding ECL signal recorded (B). a: Column electrode 1.20 V, row electrode open; b: Column electrode 1.2 V, row electrode −1.3 V; c: Column electrode 1.2 V, row electrode open. $Ru(bpy)_3^{2+}$: 8.0×10^{-8} mol L^{-1}.

it can be seen that only oxidation and reduction potentials have been applied on the crossing electrodes, the ECL signal could be detected. And the detection current can be enhanced also based on redox-cycling.

The relationship between the ECL intensity and the gap has also been studied. The results showed that the ECL intensity decreased significantly with increasing distance. The same results can be found on the current amplification. We also found that if the distance was larger than 150 μm, only a weak ECL signal could be detected, the reasons might be due to the fact that the distance was outside the region of the expected diffusion layer, so $Ru(bpy)_3^{3+}$ and $Ru(bpy)_3^{+}$ had very little chance of meeting together to produce ECL.

By applying the appropriate potential on the micro-electrodes, we sequentially detected the ECL from different addressing points. The results are shown in Fig. 4(A), the ECL intensities at each point showed good reproducibility, the deviation was lower than 5%, which indicated that it was easy to solve the problem of poor reproducibility in ECL detection by this method. We partly covered two addressing points with 5 μm-thick SU-8, since the oxidation of $Ru(bpy)_3^{2+}$ had been blocked, no ECL signals had been detected. If we addressed two points at the same time, the ECL intensity would be double too. These results also indicated that no cross talking happened between the neighbor points. If a transparent material, such as ITO was used as the working electrode, and a sensitive CCD camera was used for detection of ECL signal, the separated points on the chip might be detected simultaneously.

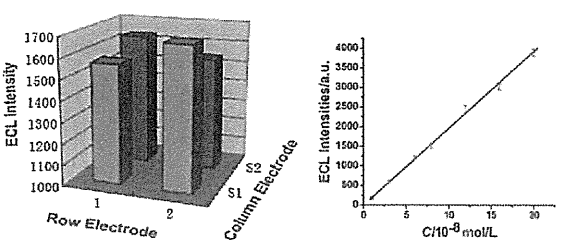

Fig. 4 (A) ECL intensities of 8.0×10^{-8} mol L^{-1} $Ru(bpy)_3^{2+}$ recorded at four different addressing points. (B) The relationship between ECL intensity and $Ru(bpy)_3^{2+}$ concentration.

The ECL intensity at each addressable point was found to be linear with the concentration of $Ru(bpy)_3^{2+}$ in the range of 1×10^{-8}–2×10^{-7} mol L^{-1} with a detection limit of 4×10^{-9} mol L^{-1} (shown in Fig. 4(B)).

In summary, this is the first report of an addressable ECL detection system based on the redox-cycling system. The detection can be performed in a 'direct way' without adding any co-reactant. The device is simple but can provide ECL responses with redox-cycling at each addressable point easily. Though the system developed in this study was carried out in an organic solution, it can also be carried out in aqueous medium, which makes is possible to develop immunoassays involving redox-cycling type ECL as the detection principle.

This study was supported by the National Basic Research Program of China (No. 2010CB732403), the NSFC (20735002, 20905013), and partly supported by Special Coordination Funds for Promoting Science and Technology, Formation of Innovation Center for Fusion of Advanced Technologies, from Japan Science and Technology Agency, and by a Grant-in-Aid (445) for Science Research on Priority Areas "Life Surveyor" from MEXT, Japan. Z.Y also thanks to the support of the Special Foundation for Young Scientists of Fujian Province, China (2008F3057).

Notes and references

1 D. M. Hercules and F. E. Lytle, *J. Am. Chem. Soc.*, 1966, **88**, 4745.
2 N. E. Tokel and A. J. Bard, *J. Am. Chem. Soc.*, 1972, **94**, 2862–2863.
3 I. Rubinstein and A. J. Bard, *J. Am. Chem. Soc.*, 1981, **103**, 512–516.
4 A. W. Knight and G. M. Greenway, *Analyst*, 1996, **121**, 101R–106R.
5 M. M. Richter, *Chem. Rev.*, 2004, **104**, 3003–3036.
6 N. E. Tokel-Takvoryan, R. E. Hemangway and A. J. Bard, *J. Am. Chem. Soc.*, 1973, **95**, 6582–6589.
7 J. E. Bartelt, S. M. Drew and R. M. Wightman, *J. Electrochem. Soc.*, 1992, **139**, 70–74.
8 X. X. Yan, H. Li, Z. H. Xu and W. S. Li, *Bioelectrochemistry*, 2009, **74**, 310–314.
9 C. E. Chidsey, B. J. Feldman, C. Lundgren and R. W. Murry, *Anal. Chem.*, 1986, **58**, 601–607.
10 K. M. Maness, R. H. Terrill, T. J. Meyer, R. W. Murray and R. M. Wightman, *J. Am. Chem. Soc.*, 1996, **118**, 10609–10616.
11 K. Ide, M. Fujimoto, T. Kado and S. Hayase, *J. Electrochem. Soc.*, 2008, **155**, B645–B649.
12 P. E. Michel, N. F. Rooij, M. Koudelka-Hep, K. A. Fahnrich, C. K. O'Sullivan and G. G. Guilbault, *J. Electroanal. Chem.*, 1999, **474**, 192–194.
13 A. Chovin, P. Carrigue, P. Vinatier and N. Sojic, *Anal. Chem.*, 2004, **76**, 357–364.
14 Z. Y. Lin, Y. Takahashi, Y. Kitagawa, T. Umemura, H. Shiku and T. Matsue, *Anal. Chem.*, 2008, **80**, 6830–6833.
15 Z. Y. Lin, Y. Takahashi, T. Murata, M. Takeda, K. Ino, H. Shiku and T. Matsue, *Angew. Chem., Int. Ed.*, 2009, **48**, 2044–2046.

Myomectomy reduces endometrial T2 relaxation times

Magnetic resonance imaging was used to measure the endometrial T2 relaxation times of patients with infertility with fibroma. Although the location of fibromas did not influence the T2 relaxation times, we did observe a significant decrease in endometrial T2 relaxation times after myomectomy. (Fertil Steril® 2011;■:■–■. ©2011 by American Society for Reproductive Medicine.)

Key Words: MRI, T2 relaxation time, fibroid, myomectomy, endometrium

Although uterine fibroids, which occur in 20% to 50% of women, are the most common type of solid pelvic tumor (1), the relationship between fibroids and infertility is not well established (2, 3). It has been reported that myomectomy can increase the pregnancy rate for patients with infertility (4). However, the mechanisms by which this occurs are not well understood. Several theories have been proposed. First, it is possible that fibroids alter uterine cavity contour, resulting in mechanical pressure. Alternatively, the fibroids may induce abnormal uterine contractility (5, 6). Finally, local inflammation associated with the presence of fibroids may give rise to a hostile endometrial environment that impairs sperm transport and embryo implantation (5). It has been reported that excessive concentrations of inflammatory cytokines have deleterious effects on embryonic development and implantation (7, 8). Inagaki et al. (9) demonstrated that uterine cavities containing fibroids exhibit a state of excess inflammation, with up-regulation of matrix metalloproteinases and inflammatory cytokines such as interleukin-1 and tumor necrosis factor α.

Magnetic resonance imaging (MRI) is a high-resolution method of differentiating soft tissues. In MRI, the nuclei of atoms in samples first are aligned along a static magnetic field, then are excited to a higher-energy state by a radiofrequency signal, and then return to a lower-energy equilibrium state. T2 relaxation time is a parameter that describes the relaxation to the equilibrium state once the radiofrequency signal is turned off. As an assessment of inflammatory status, T2 relaxation time is a useful way to detect the inflammatory status of rheumatoid disease (10, 11), dermatomyositis (12), and Graves' orbitopathy in Graves' disease (13, 14). In the present study, we investigated the endometrial T2 relaxation times of patients with infertility with fibroma. We compared T2 relaxation times before and after surgery to examine the effect of myomectomy on the endometrium of patients with uterine fibroids.

A total of 35 patients with uterine fibroids who desire pregnancy were examined by MRI between September 2008 and October 2010 at Takinogawa Clinic. Inclusion criteria were as follows. First, patients had intramural- or submucosal-type fibroid. Second, in advance of MRI all patients underwent screening for ovulation and corpus luteum function. Patients had regular menstrual cycles of approximately 28 days. Basal levels of serum FSH, LH, and PRL on menstrual cycle day 3 through 5 were within normal range (criteria: FSH 3.5–12.5 mIU/mL, LH 2.4–12.6 mIU/mL, and PRL 4.9–29.3 ng/mL). Serum E_2 and P concentration in midluteal phase were >100 pg/mL and 10 ng/mL, respectively. After the screening test, ovarian functional status was monitored by basal body temperature (BBT) chart. An analysis was performed of BBT graphs, in which a rise in temperature of at least 0.2°C above that of the preceding 6 days that was completed in <48 hours and sustained for at least 11 days would indicate the occurrence of ovulation (15). All patients included in this study showed unequivocal biphasic cycles in their BBT chart. We designated the first day showing elevated temperature of at least 0.2°C as luteal phase day 1. Third, MRI was performed during the time of implantation window (luteal phase day 5–day 9), judged retrospectively by BBT chart (judged by gynecologists O.Y. and H.T.).

Osamu Yoshino, M.D., Ph.D.[a,b]
Masaaki Hori, M.D., Ph.D.[c]
Yutaka Osuga, M.D., Ph.D.[a]
Toshihiko Hayashi, M.D., Ph.D.[d]
Yoko Sadoshima, M.D.[b]
Hiroko Tsuchiya, M.D.[b]
Osamu Nishii, M.D., Ph.D.[b]
Yuji Taketani, M.D., Ph.D.[a]

[a] *Department of Obstetrics and Gynecology, University of Tokyo, Tokyo, Japan*
[b] *Department of Obstetrics and Gynecology, Mizonokuchi Hospital, Teikyo University, Kawasaki, Kanagawa, Japan*
[c] *Department of Radiology, Juntendo University, Tokyo, Japan*
[d] *Department of Radiology, Mizonokuchi Hospital, Teikyo University, Kawasaki, Kanagawa, Japan*

Received December 16, 2010; revised December 29, 2010; accepted January 7, 2011.
O.Y. has nothing to disclose. M.H. has nothing to disclose. Y.O. has nothing to disclose. T.H. has nothing to disclose. Y.S. has nothing to disclose. H.T. has nothing to disclose. O.N. has nothing to disclose. Y.T. has nothing to disclose.
Supported by Health and Labor Sciences Research Grants from the Ministry of Health, Labor, and Welfare of Japan and a Grant-in-Aid for Scientific Research from the Ministry of Education, Culture, Sports, Science, and Technology.
Reprint requests: Osamu Yoshino, M.D., Ph.D., and Yutaka Osuga, M.D., Ph.D., Department of Obstetrics and Gynecology, University of Tokyo, 7-1-3 Hongo, Bunkyo-ku, Tokyo 113-8655, Japan (E-mail: oyoshino624@hotmail.co.jp; yutakaos-tky@umin.ac.jp).

By routine MRI study, the information retrieved included the location, number, and size of fibroids. Magnetic resonance studies were performed with use of a 1.5-T magnet unit (MRI machine from Siemens Japan, Shinagawa, Japan). Subsequently, conventional axial and sagittal T2–weighted images (repetition time [TR]/echo time [TE] = 4560–4720/107–111 milliseconds) and axial T1–weighted images (TR/TE = 550/8.5 milliseconds) were obtained with use of fast spin-echo techniques. T2 relaxation times of endometrium were measured on the same slice (350-mm field of view, 132 × 192 matrix, 3-mm slice thickness, bandwidth 362 Hz) with use of a spin-echo sequence. Eight images were acquired at each of the following TEs: 1.7, 23.4, 35.1, 46.8, 58.5, 70.2, 81.9, 93.6, 105.3, 117, and 128 milliseconds. The TR was 3 seconds, giving a total of 509 seconds acquisition time.

Ten out of 35 patients underwent myomectomy at Teikyo Mizonokuchi hospital. Among these 10 patients, 9 patients underwent laparoscopic-assisted myomectomy, and 1 patient underwent transcervical resection of fibroma. Four to 6 months after surgery, patients underwent a second MRI to evaluate T2 relaxation times during the implantation window. For statistical analysis, the Mann-Whitney *U* test was used for comparing between groups, and the paired *t*-test was used for comparing results before and after surgery.

T2 relaxation times in uterine endometrium obtained from patients with infertility who had intramural-type (n = 24) and submucosal-type (n = 12) fibroids were compared. We examined data from the midluteal phase. As shown in Figure 1A, the median value and minimum to maximum data of the two groups were 213 milliseconds (99–368 milliseconds) and 187 milliseconds (111–455 milliseconds) in intramural fibroids and submucosal fibroids, respectively. There was no statistical difference between groups (P=.9).

Because T2 relaxation times in the endometrium were comparable between intramural and submucosal fibroids (Fig. 1A), the data from both groups were combined in the subsequent study. After myomectomy, 10 patients underwent MRI at midluteal phase, and T2 relaxation times in the endometrium before and after surgery were compared. Of the 10 patients, 7 underwent surgery for intramural-type fibroids, and 3 underwent surgery for submucosal-type fibroids. As shown in Figure 1B, T2 relaxation times were decreased significantly after surgery (P=.03).

In the present study, we investigated the endometrial T2 relaxation times of patients with infertility with fibroma. We found that the endometrial T2 relaxation times were comparable regardless of the location of fibromas. Moreover, endometrial T2 relaxation times obtained after myomectomy were shortened significantly compared with the results before surgery.

Management of fibroids continues to present difficulties when used to treat infertility, because of a lack of understanding of the mechanisms by which fibroids impede pregnancy. Although myomectomy is recognized as a method to increase the rate of pregnancy (4), the precise mechanism of its contribution to fertility remains uncertain. It has been reported that the local inflammation associated with the presence of fibroids may result in a hostile endometrial environment that impairs fertility (7–9). Inagaki et al. (9) proved that the uterine cavities of patients with fibroids exhibited excessive inflammatory status. Accordingly, myomectomy might increase the fertility rate by decreasing the inflammatory status of the endometrium. In that study, 5 mL of saline solution was injected into the uterine cavity, and matrix metalloproteinase and cytokine levels of the fluid were measured to determine the inflammatory status directly (9). However, the volume of the uterine cavity can be decreased after removal of fibroids, making it difficult to compare precisely the inflammatory status before and after surgery. Therefore, it is necessary to develop less-invasive techniques that can estimate the inflammatory status of the uterine cavity. In the present study, we focused on T2 relaxation times obtained by MRI. This technique has proved useful in detecting the inflammatory activity of rheumatoid disease (10, 11), dermatomyositis (12), and Graves' orbitopathy in Graves' disease (13). Here, we observed a significant decrease in T2 relaxation times in patients examined after myomectomy. This suggests that myomectomy may suppress inflammatory activity in the endometrium.

FIGURE 1

(**A**) T2 relaxation times in uterine endometrium obtained from patients with infertility who had intramural-type (n = 24) and submucosal-type (n = 12) fibroids were compared. The data from the midluteal phase were examined. (**B**) Ten patients underwent myomectomy and received MRI examination at the midluteal phase before and after surgery. T2 relaxation times in the endometrium were compared P=0.03.

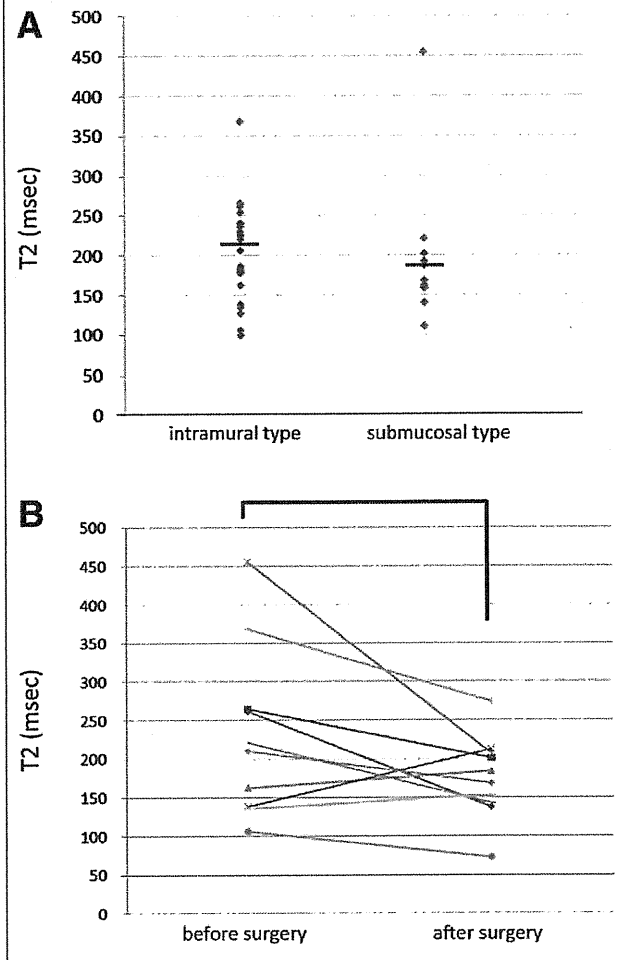

Yoshino. Correspondence. Fertil Steril 2011.

T2 relaxation times in the human endometrium have been examined throughout the menstrual cycle. Varpula et al. (16) reported that a rapid increase in T2 relaxation times occurred during the proliferative phase, followed by little or no increase through the middle of the secretory phase. Hoad et al. (17) also reported that, during the periovulatory phase, T2 relaxation times were longer than in the other phases. They also observed that the variation in uterine tissue relaxation times between subjects was greater than the intrasubject cycle variation. Because of the large "normal" range, it might be very difficult to compare subjects or determine pathologic changes in the tissues from just a single measurement. However, because individuals exhibited similar increases and decreases over the menstrual cycle, the changes in T2 relaxation times within the same subject can be evaluated (17). Therefore, by comparing T2 relaxation times at the same menstrual phase obtained before and after myomectomy, the effect of surgery could be estimated. In our experiment, T2 relaxation times were measured during the "implantation window," the luteal phase day 5 to 9. We observed that there is no significant difference in T2 relaxation times between patients with fibroma and healthy volunteers (data not shown). Thus, measurement of T2 relaxation times would not be an effective way to detect uterine abnormalities, but it can be used to assess the success of myomectomy and is valuable in increasing our understanding of the pathophysiology of uterine fibroids in infertility. Other than inflammation (12, 14), iron content (18) is also known to increase T2 relaxation times. Therefore, further study is needed to confirm that T2 changes after myomectomy actually represent the change of inflammatory status in endometrium. This work represents a first step toward better understanding the relationship between T2 relaxation times and uterine fibroids in patients with infertility.

Acknowledgments: The authors thank Heather M. Martinez, Ph.D., for her helpful discussion and critical reading of the manuscript. They thank Yasufumi Shimizu, Ph.D., M.D., Kouji Motoyama, Ph.D., M.D., and Yasuhiro Kawamura, Ph.D., M.D. (Denentoshi Ladies' Clinic); Kenichi Tatsumi, Ph.D., M.D. (Umegaoka Women's Clinic); Susumu Tokuoka, Ph.D., M.D. (Tokuoka Women's Clinic); Ryo Matsuoka, Ph.D., M.D. (Tokyo Hitachi Hospital); and Takayoshi Ogawa, Ogawa, Ph.D., M.D. (Ogawa Clinic) for their supporting this study. They also thank Mr. Ryuji Nojiri and Mr. Yoshitsugu Funatsu (Takinogawa Clinic) for their technical assistance.

REFERENCES

1. Verkauf BS. Myomectomy for fertility enhancement and preservation. Fertil Steril 1992;58:1–15.
2. Donnez J, Jadoul P. What are the implications of myomas on fertility? A need for a debate? Hum Reprod 2002;17:1424–30.
3. Somigliana E, Vercellini P, Daguati R, Pasin R, De Giorgi O, Crosignani PG. Fibroids and female reproduction: a critical analysis of the evidence. Hum Reprod Update 2007;13:465–76.
4. Bulletti C, De Ziegler D, Polli V, Flamigni C. The role of leiomyomas in infertility. J Am Assoc Gynecol Laparosc 1999;6:441–5.
5. Richards PA, Richards PD, Tiltman AJ. The ultrastructure of fibromyomatous myometrium and its relationship to infertility. Hum Reprod Update 1998;4:520–5.
6. Yoshino O, Hayashi T, Osuga Y, Orisaka M, Asada H, Okuda S, et al. Decreased pregnancy rate is linked to abnormal uterine peristalsis caused by intramural fibroids. Hum Reprod 2010;25:2475–9.
7. Inoue T, Kanzaki H, Iwai M, Imai K, Narukawa S, Higuchi T, et al. Tumour necrosis factor alpha inhibits in-vitro decidualization of human endometrial stromal cells. Hum Reprod 1994;9:2411–7.
8. Kariya M, Kanzaki H, Takakura K, Imai K, Okamoto N, Emi N, et al. Interleukin-1 inhibits in vitro decidualization of human endometrial stromal cells. J Clin Endocrinol Metab 1991;73:1170–4.
9. Inagaki N, Ung L, Otani T, Wilkinson D, Lopata A. Uterine cavity matrix metalloproteinases and cytokines in patients with leiomyoma, adenomyosis or endometrial polyp. Eur J Obstet Gynecol Reprod Biol 2003;111:197–203.
10. Kight AC, Dardzinski BJ, Laor T, Graham TB. Magnetic resonance imaging evaluation of the effects of juvenile rheumatoid arthritis on distal femoral weight-bearing cartilage. Arthritis Rheum 2004;50:901–5.
11. Gasson J, Gandy SJ, Hutton CW, Jacoby RK, Summers IR, Vennart W. Magnetic resonance imaging of rheumatoid arthritis in metacarpophalangeal joints. Skeletal Radiol 2000;29:324–34.
12. Maillard SM, Jones R, Owens C, Pilkington C, Woo P, Wedderburn LR, et al. Quantitative assessment of MRI T2 relaxation time of thigh muscles in juvenile dermatomyositis. Rheumatology (Oxford) 2004;43:603–8.
13. Utech CI, Khatibnia U, Winter PF, Wulle KG. MR T2 relaxation time for the assessment of retrobulbar inflammation in Graves' ophthalmopathy. Thyroid 1995;5:185–93.
14. Hosten N, Sander B, Cordes M, Schubert CJ, Schorner W, Felix R. Graves ophthalmopathy: MR imaging of the orbits. Radiology 1989;172:759–62.
15. Ayres-de-Campos D, Silva-Carvalho JL, Oliveira C, Martins-da-Silva I, Silva-Carvalho J, Pereira-Leite L. Inter-observer agreement in analysis of basal body temperature graphs from infertile women. Hum Reprod 1995;10:2010–6.
16. Varpula M, Komu M, Irjala K. Relaxation time changes of the uterus during the menstrual cycle: correlation with hormonal status. Eur J Radiol 1993;16:90–4.
17. Hoad CL, Fulford J, Raine-Fenning NJ, Campbell BK, Johnson IR, Gowland PA. In vivo perfusion, T1, and T2 measurements in the female pelvis during the normal menstrual cycle: a feasibility study. J Magn Reson Imaging 2006;24:1350–6.
18. Argyropoulou MI, Metafratzi Z, Kiortsis DN, Bitsis S, Tsatsoulis A, Efremidis S. T2 relaxation rate as an index of pituitary iron overload in patients with beta-thalassemia major. AJR Am J Roentgenol 2000;175:1567–9.

High Mobility Group Box 1 (HMGB1) Levels in the Placenta and in Serum in Preeclampsia

Bo Wang*, Kaori Koga, Yutaka Osuga, Tetsuya Hirata, Ako Saito, Osamu Yoshino, Yasushi Hirota, Miyuki Harada, Yuri Takemura, Tomoyuki Fujii, Yuji Taketani

Department of Obstetrics and Gynecology, University of Tokyo, Tokyo, Japan

Keywords
Apoptosis, hypoxia, inflammation, oxidative stress, receptor for advanced glycation end products, toll-like receptors

Correspondence
Kaori Koga, Department of Obstetrics and Gynecology, University of Tokyo, 7-3-1 Hongo Bunkyo, Tokyo 113-8655, Japan.
E-mail: kawotan-tky@umin.ac.jp

*Present address: Obstetrics and Gynecology, Women's Hospital, School of Medicine, Zhejiang University, Zhejiang, China.

Submitted October 4, 2010;
accepted December 13, 2010.

Citation
Wang B, Koga K, Osuga Y, Hirata T, Saito A, Yoshino O, Hirota Y, Harada M, Takemura Y, Fujii T, Taketani Y. High mobility group Box 1 (HMGB1) levels in the placenta and in serum in preeclampsia. Am J Reprod Immunol 2011

doi:10.1111/j.1600-0897.2010.00975.x

Problem
Preeclampsia is a pregnancy disorder characterized by systemic inflammation. High mobility group box 1 (HMGB1) is a molecule known to act as a 'danger signal' by participating in various inflammatory processes, but data in regard to preeclampsia are sparse. The aim of this study was to analyze placental and serum HMGB1 levels in normal pregnancy and preeclampsia.

Method of study
Sera were collected from women with preeclampsia soon after the manifestation of the disease and before commencing any medication. Placental samples were collected immediately after delivery. Expressed isoforms of HMGB1 (28- and 30-kDa) in the placenta were evaluated by Western blot analysis. Serum HMGB1 concentrations were measured using enzyme-linked immunosorbent assays (ELISA).

Results
Two isoforms of HMGB1 are expressed by the human placenta. The 28- and 30-kDa HMGB1 isoforms were expressed highly in preeclamptic placental tissue; however, compared with normotensive control tissue, differences in detected expression levels did not reach statistical significance. No significant difference was observed in serum HMGB1 levels between control and preeclampsia.

Conclusion
Inflammation provoked by HMGB1 is likely to be involved in the proinflammatory process in preeclamptic placenta. Further studies are needed to elucidate the precise role of HMGB1 in preeclampsia.

Introduction

Preeclampsia is a placenta-originated disorder and affects 3–5% of all pregnancies. It remains as one of the leading contributors to maternal and fetal morbidity and mortality.[1] It is a disorder characterized by intravascular inflammation and endothelial cell dysfunction. Despite recent progress in research, the biology of preeclampsia is still poorly understood.[2]

High mobility group box 1 (HMGB1), a non-histone chromatin-associated protein, was discovered three decades ago as a nuclear protein that migrates quickly during electrophoresis and was named according to this property.[3] HMGB1 is released from damaged cells and acts as a 'danger signal' by

participating in various inflammatory processes, including maturation of immune cells, release of cytokines and other inflammatory mediators, and tissue remodeling.[4,5] HMGB1 mediates its inflammatory responses by signaling via receptors such as the receptor for advanced glycation end products (RAGE)[6] and toll-like receptor (TLR) 2 and TLR4.[7] Ligation for these receptors results in activation of nuclear factor kappa B (NFκB), which induces upregulation of leukocyte adhesion molecules and the production of proinflammatory cytokines in both hematopoietic and endothelial cells, thereby promoting inflammation.

It has been demonstrated that HMGB1 is involved in the pathogenesis of a variety of both infectious and non-infectious inflammatory conditions. Elevated levels of HMGB1 in serum and tissues are observed during infection and tissue injury, and targeting HMGB1 with specific antagonists can have protective effects in established inflammatory diseases. For instance, circulating HMGB1 levels are markedly increased during severe sepsis,[8] pneumonia,[9] systemic lupus erythematosis,[10] and in the synovial fluid of patients with rheumatoid arthritis.[11] Administration of HMGB1 antagonists has been reported to decrease organ damage and mortality in models of systemic inflammation such as sepsis,[12,13] brain infarction,[14] arthritis,[15] acute pancreatitis,[16] and lung inflammation.[17]

Preeclampsia is characterized by an inflammatory state that includes elevated levels of proinflammatory molecules in the placenta and maternal serum.[18] The expression of RAGE, one of the receptors for HMGB1, was reported to be significantly higher in preeclamptic placenta when compared with normal placental tissue.[19,20] TLR4, also a receptor for HMGB1, is expressed higher in trophoblasts from patients with preeclampsia compared to normal pregnancies.[21,22] As for HMGB1, Holmlund et al.[23] demonstrated its expression in the trophoblasts by immunohistochemistry. Further immunohistochemical analysis demonstrated higher expression levels of cytoplasmic HMGB1 in the decidua from women with preeclampsia compared with normal pregnancy, but the difference was not conclusive in trophoblasts.[23] The circulating level of HMGB1 in pregnant women has never been elucidated.

In this study, we measured HMGB1 levels in the placenta and serum in normal pregnancies and pregnancies complicated by preeclampsia to ascertain whether this molecule is involved in the pathogenesis of preeclampsia.

Materials and methods

Serum and Tissue Collection

The study was approved by the ethical committee of the University of Tokyo and Musashino Red Cross Hospital, and written informed consent was obtained from all women. Placentas and maternal venous blood were obtained from women with uncomplicated, normotensive pregnancies and pregnancies complicated by preeclampsia. Preeclampsia was diagnosed by the presence of hypertension (an absolute blood pressure ≥140 mmHg systolic and/or 90 mmHg diastolic after 20 weeks of gestation) with proteinuria (≥300 mg/24-hr). Patients with preeclampsia did not have any prior history of hypertension or renal disease. All women in control group did not show clinical or pathological signs of preeclampsia, infections, or any other maternal or placental disease.

Blood samples were collected from women with preeclampsia soon after the manifestation of the disease and before commencing any medication. Sera were separated by centrifugation and stored at −70°C before use. Placental samples were collected immediately after delivery. Placental tissue was taken from the middle part of the placenta to avoid amnion and decidual tissue contamination. All samples were stored at −70°C until assayed.

Western Blot Analysis

Placental tissues were homogenized and then sonicated in lysis buffer [10 mM Tris–HCl, 50 mM NaCl, 2 mM EDTA, 1% Triton X-100, (pH 7.0)] with protease inhibitor cocktail (Roche Diagnostics GmbH, Mannheim, Germany). The protein concentration was determined using a modified Bradford protein assay with bovine serum albumin (Sigma-Aldrich, St Louis, MO, USA) as a standard. Thirty micrograms of protein was separated on 12.5% sodium dodecyl sulfate polyacrylamide electrophoresis gel and then transferred onto polyvinylidene fluoride (PVDF) transfer membranes (Amersham Biosciences, Piscataway, NJ, USA). Protein extracted from human endometrium was used as a positive control.[24] The blots were blocked in tris-buffered saline – 0.1% Tween-20 containing 5% nonfat milk and then incubated with antibodies at 4°C overnight. The membranes were incubated with primary antibodies: anti-human HMGB1 antibody (final concentration 2 μg/mL; R & D

systems, Minneapolis, MN, USA) or goat anti-human actin antibody (1/1000; Santa Cruz Biotechnology, Inc. Santa Cruz, CA, USA) as a loading control. Normal mouse IgG2B (Amersham Biosciences, Little Chalfont, UK) was used as an isotype control. The secondary antibody was horseradish peroxidase-conjugated anti-mouse (1/1000; Amersham Biosciences) or anti-goat (1/5000; Santa Cruz) IgG, which was incubated for 1 hr at room temperature. Signals were developed using ECL Western blotting system (Amersham Biosciences). Densitometric analysis was performed using ImageJ Image Software (National Institutes of Health, Bethesda, MD, USA). Each HMGB1 band was normalized to the densitometric value obtained from the same lane by blotting for actin, the internal reference.

Enzyme-linked Immunosorbent Assay (ELISA) Measurement of HMGB1

The concentration of HMGB1 in serum was measured in duplicate by a specific ELISA kit (Shino-test Corporation, Kanagawa, Japan). The minimum detectable dose of HMGB1 was 1 ng/mL. The intra- and inter-assay coefficients of variation were all <10%.

Statistical Analysis

Data analysis was performed using the statistical software package SPSS for Windows (Chicago, IL, USA). All data were checked for their normal distribution by submission to the Kolmogorov–Smirnov test, and if significant, non-parametric statistical analysis was applied. Parametric variables underwent the Student's *t*-test. Statistical significance was considered as $P < 0.05$.

Results

We firstly analyzed HMGB1 expression in the placenta. Western blot analysis showed that the human term placenta expresses HMGB1 and is detected as a 28- and 30-kDa band corresponding to two distinct isoforms of the molecule (Fig. 1). The latter band corresponds to biologically active acetylated isoform.[5,24]

We then compared the placental expression levels of the two isoforms between normal pregnancy and pregnancy complicated by preeclampsia. Maternal age, gestational age, parity, and mode of in delivery were comparable in both groups (Table I). Compared

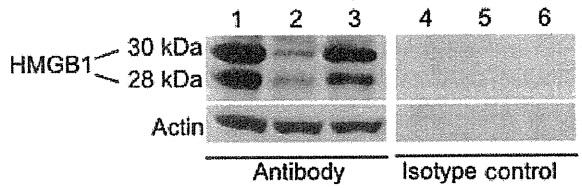

Fig. 1 A representative result of Western blot analysis in the placenta in preeclampsia (1, 4), normal pregnancy (2, 5) and human endometrium as a positive control (3, 6) for anti-high mobility group box 1 (HMGB1) or anti-actin antibody (1, 2, 3) and isotype negative control (4, 5, 6). Note there are two bands (28- and 30-kDa) specific for HMGB1.

Table I Clinical Backgrounds and Serum High Mobility Group Box 1 (HMGB1) Concentrations in Women With or Without Preeclampsia

	Normal pregnancy ($n = 32$)	Preeclampsia ($n = 35$)	*P*
Maternal age, year*	32.94 ± 3.58	33.49 ± 4.09	NS
Gestational age, week*	34.40 ± 4.90	33.50 ± 4.78	NS
HMGB1, ng/mL			
Median (IQR)	4.757 (2.592–6.861)	4.312 (2.451–6.011)	
Mean ± S.D.	5.119 ± 2.773	4.511 ± 2.537	NS

IQR, interquartile range.
*Data are presented as mean ± S.D.

to normal pregnancy, the level of 28- and 30-kDa HMGB1 expression was higher in preeclampsia, especially in the 28-kDa isoform (normal versus preeclampsia: 0.176 ± 0.112 versus 0.363 ± 0.296, 0.463 ± 0.332 versus 0.581 ± 0.379; 28-, 30-kDa, respectively: mean ± S.D.), although the difference did not reach statistical significance ($P = 0.087$, $P = 0.471$; 28-, 30-kDa, respectively) (Fig. 2, Table II).

Secondly, we measured the level of serum HMGB1 in normal pregnancy and pregnancy complicated with preeclampsia. As shown in Table II, maternal age and gestational age were comparable between the normal and preeclampsia group. When we compared serum HMGB1 concentrations, there was no significant difference between controls and women with preeclampsia.

Fig. 3 shows the correlation between serum HMGB1 concentration and gestational ages for both groups. There was no correlation between gestational

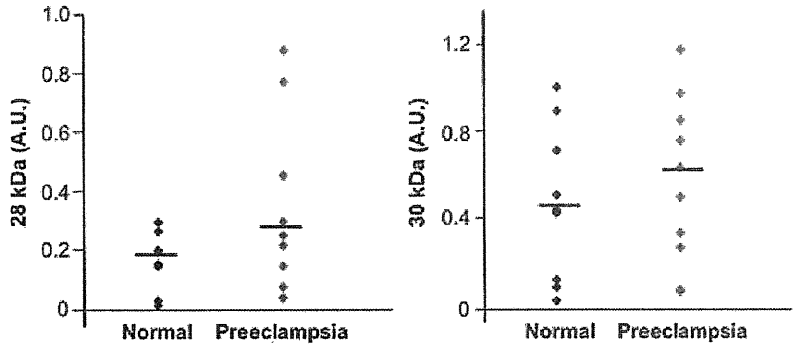

Fig. 2 A scatter plot of placental high mobility group box 1 (HMGB1) protein expression level in both 28- and 30-kDa bands in normal pregnancy and pregnancy complicated with preeclampsia. The data are presented as arbitrary densitometric units (A.U.). The horizontal bars indicate the mean. The expression level of HMGB1 protein in both isoforms was higher in preeclampsia, although the difference did not reach statistical significance ($P = 0.087$, $P = 0.471$; 28-, 30-kDa, respectively).

Table II. Clinical Backgrounds and Placental High Mobility Group Box 1 (HMGB1) Expression Levels in Women With or Without Preeclampsia

	Normal pregnancy ($n = 10$)	Preeclampsia ($n = 10$)	P
Primigravid (n)	7	7	NS[a]
Maternal age, year*	30.00 ± 5.14	33.40 ± 3.69	NS[b]
Gestational age, week*	38.81 ± 1.18	36.20 ± 3.26	NS[b]
Vaginal delivery (n)	7	3	NS[a]
HMGB1 28 kDa (A.U.)*	0.176 ± 0.112	0.363 ± 0.296	NS[b]
HMGB1 30 kDa (A.U.)*	0.463 ± 0.332	0.581 ± 0.379	NS[b]

*Data are presented as mean ± S.D.
[a]Fisher's Exact test.
[b]Student's t-test.

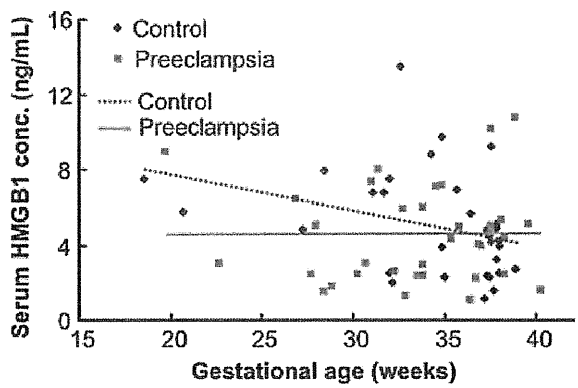

Fig. 3 A scatter plot of serum high mobility group box 1 (HMGB1) levels versus gestational age (weeks) in normal pregnancy (blue diamond dots) and women with preeclampsia (pink square dots). No statistically significant correlation was found between gestational age and serum HMGB1 level in either normal pregnancy (broken line; $r = -0.338$, $P = 0.058$) or women with preeclampsia (unbroken line; $r = 0.002$, $P = 0.993$).

age and serum HMGB1 level in normal pregnancies (Pearson correlation, $r = -0.338$, $P = 0.058$) or in women with preeclampsia ($r = 0.002$, $P = 0.993$).

Discussion

In the present study, we showed that the expression of HMGB1 in the placenta was higher in preeclampsia compared with normal pregnancy, although the difference did not reach statistical significance. There was no difference in serum HMGB1 levels between groups. These findings add to our understanding of the possible involvement of HMGB1 in the pathology of preeclampsia.

Firstly, a quantitative evaluation of HMGB1 expression in the placenta by Western blot demonstrated that the expression of 28- and 30-kDa isotypes in the placenta from women with preeclampsia was higher compared to healthy pregnancies, although the difference did not reach statistical significance. A variety of factors are reported to induce the expression of HMGB1 such as necrosis,[25] apoptosis,[26] oxidative stress,[27] and hypoxia,[15] which are all known to be enhanced in the placenta in preeclampsia. Therefore, we speculate that the expression of HMGB1 is increased in the damaged preeclamptic placenta as a 'danger signal', further enhancing the immune response.

Given the observation that placental HMGB1 is higher in preeclampsia, together with the fact that its receptors, RAGE and TLR4, are upregulated in the placenta in preeclampsia,[19,20,22,28] we suggest that the proinflammatory axis provoked by HMGB1 is enhanced in the preeclamptic placenta. Indeed, changes that may be induced by HMGB1 include NFκB activation, followed by the production of pro-inflammatory cytokines such as TNF alpha,[29] IL-6,[30] and endothelin,[31] or induction of apoptosis[32,33] are all events observed in the preeclamptic placenta. Although other endogenous and exogenous factors besides HMGB1 may also bind to RAGE and TLRs, such as advanced glycation end products (AGE) to RAGE, lipopolysaccharides and heat-shock protein 70 to TLR4, or peptidoglycan to TLR2, our result suggests that HMGB1 is one of the contributors modulating the development of preeclampsia.

There are several explanations for the lack of significant difference in placental HMGB1 levels between preeclampsia and control. Firstly, the sample number in this study was so small that the statistical study was underpowered. It is also possible that Western blotting followed by densitometry analysis has a limitation in detecting subtle difference. Another explanation could be that even in the healthy condition, the placenta is exposed by a mild inflammation, which is a nature of normal pregnant uterine environment,[34] and HMGB1 is constitutively expressed regardless of whether healthy or preeclamptic condition.

We then measured the circulating levels of HMGB1 in pregnancy. Our observation that placental HMGB1 is slightly higher in preeclampsia, and given a greater amount of trophoblast fragments are detected in the maternal circulation in preeclampsia compared to normal pregnancy,[35] prompted us to hypothesize that the circulating level of HMGB1 is higher in preeclampsia. Contrary to our hypothesis, there was no difference in the serum level of HMGB1 between normal pregnancy and pregnancy complicated by preeclampsia. One explanation could be that the level of circulating HMGB1 does not reflect its release from the placenta. This is partially supported by our finding that serum HMGB1 levels did not positively correlate with gestational age, yet HMGB1 levels should be in proportion to placental size and the number of shedding trophoblasts entering the maternal circulation. It is also possible that some component present in serum may bind HMGB1 and interfere with the ELISA system, as reported by Urbonaviciute et al.[10] Indeed, this interference resulted in an underestimation of serum HMGB1 levels in rheumatoid arthritis.[36] In addition, soluble RAGE (sRAGE), which is reported to capture and eliminate circulating HMGB1,[37] may have affected our results because circulating sRAGE levels are known to be elevated in preeclampsia.[28] Therefore, our results do not exclude the possibility that circulating HMGB1 is elevated in preeclampsia and could be a therapeutic target for preeclampsia.

In summary, we have demonstrated that the levels of HMGB1 in the placenta were slightly higher in preeclampsia. Inflammation provoked by HMGB1 is likely to be involved in the proinflammatory event, which is a prominent feature found in preeclamptic placenta. Further studies are needed to elucidate the precise role of HMGB1 in preeclampsia.

Acknowledgments

The authors thank medical colleagues in the University of Tokyo Hospital, Musashino Red Cross Hospital, for their assistance in sample collection and Dr. Kate Hale for editing the manuscript. BW is a fellow of Japan China Sasakawa Medical Fellow for YO. This work was supported by grants from Ministry of health, Labor and Welfare and Ministry of Education, Culture, Sports, Science and Technology and by grants from Japan China Medical Association (BW), Yamaguchi Endocrine Research Foundation (KK), the Japan Society for the Study of Hypertension in Pregnancy (KK), and Inohana Alumni Association of Chiba University School of Medicine (KK).

References

1 Sibai B, Dekker G, Kupferminc M: Pre-eclampsia. *Lancet* 2005; 365:785–799.
2 Carty DM, Delles C, Dominiczak AF: Novel biomarkers for predicting preeclampsia. *Trends Cardiovasc Med* 2008; 18:186–194.
3 Goodwin GH, Sanders C, Johns EW: A new group of chromatin-associated proteins with a high content of acidic and basic amino acids. *Eur J Biochem* 1973; 38:14–19.
4 Campana L, Bosurgi L, Rovere-Querini P: HMGB1: a two-headed signal regulating tumor progression and immunity. *Curr Opin Immunol* 2008; 20:518–523.
5 Bianchi ME, Manfredi AA: High-mobility group box 1 (HMGB1) protein at the crossroads between innate and adaptive immunity. *Immunol Rev* 2007; 220:35–46.
6 Hori O, Brett J, Slattery T, Cao R, Zhang J, Chen JX, Nagashima M, Lundh ER, Vijay S, Nitecki D, Morser J, Stern D, Schmidt AM: The receptor for advanced glycation end products (RAGE) is a cellular binding site for amphoterin. Mediation of neurite outgrowth and co-expression of rage and amphoterin in the developing nervous system. *J Biol Chem* 1995; 270:25752–25761.

7 Park JS, Gamboni-Robertson F, He Q, Svetkauskaite D, Kim JY, Strassheim D, Sohn JW, Yamada S, Maruyama I, Banerjee A, Ishizaka A, Abraham E: High mobility group box 1 protein interacts with multiple Toll-like receptors. *Am J Physiol Cell Physiol* 2006; 290:C917–C924.

8 Karlsson S, Pettila V, Tenhunen J, Laru-Sompa R, Hynninen M, Ruokonen E: HMGB1 as a predictor of organ dysfunction and outcome in patients with severe sepsis. *Intensive Care Med* 2008; 34:1046–1053.

9 Angus DC, Yang L, Kong L, Kellum JA, Delude RL, Tracey KJ, Weissfeld L: Circulating high-mobility group box 1 (HMGB1) concentrations are elevated in both uncomplicated pneumonia and pneumonia with severe sepsis. *Crit Care Med* 2007; 35:1061–1067.

10 Urbonaviciute V, Furnrohr BG, Weber C, Haslbeck M, Wilhelm S, Herrmann M, Voll RE: Factors masking HMGB1 in human serum and plasma. *J Leukoc Biol* 2007; 81:67–74.

11 Taniguchi N, Kawahara K, Yone K, Hashiguchi T, Yamakuchi M, Goto M, Inoue K, Yamada S, Ijiri K, Matsunaga S, Nakajima T, Komiya S, Maruyama I: High mobility group box chromosomal protein 1 plays a role in the pathogenesis of rheumatoid arthritis as a novel cytokine. *Arthritis Rheum* 2003; 48:971–981.

12 Wang H, Bloom O, Zhang M, Vishnubhakat JM, Ombrellino M, Che J, Frazier A, Yang H, Ivanova S, Borovikova L, Manogue KR, Faist E, Abraham E, Andersson J, Andersson U, Molina PE, Abumrad NN, Sama A, Tracey KJ: HMG-1 as a late mediator of endotoxin lethality in mice. *Science* 1999; 285:248–251.

13 Yang H, Ochani M, Li J, Qiang X, Tanovic M, Harris HE, Susarla SM, Ulloa L, Wang H, DiRaimo R, Czura CJ, Wang H, Roth J, Warren HS, Fink MP, Fenton MJ, Andersson U, Tracey KJ: Reversing established sepsis with antagonists of endogenous high-mobility group box 1. *Proc Natl Acad Sci U S A* 2004; 101:296–301.

14 Liu K, Mori S, Takahashi HK, Tomono Y, Wake H, Kanke T, Sato Y, Hiraga N, Adachi N, Yoshino T, Nishibori M: Anti-high mobility group box 1 monoclonal antibody ameliorates brain infarction induced by transient ischemia in rats. *FASEB J* 2007; 21:3904–3916.

15 Hamada T, Torikai M, Kuwazuru A, Tanaka M, Horai N, Fukuda T, Yamada S, Nagayama S, Hashiguchi K, Sunahara N, Fukuzaki K, Nagata R, Komiya S, Maruyama I, Fukuda T, Abeyama K: Extracellular high mobility group box chromosomal protein 1 is a coupling factor for hypoxia and inflammation in arthritis. *Arthritis Rheum* 2008; 58:2675–2685.

16 Sawa H, Ueda T, Takeyama Y, Yasuda T, Shinzeki M, Nakajima T, Kuroda Y: Blockade of high mobility group box-1 protein attenuates experimental severe acute pancreatitis. *World J Gastroenterol* 2006; 12:7666–7670.

17 Abraham E, Arcaroli J, Carmody A, Wang H, Tracey KJ: HMG-1 as a mediator of acute lung inflammation. *J Immunol* 2000; 165:2950–2954.

18 Schiessl B: Inflammatory response in preeclampsia. *Mol Aspects Med* 2007; 28:210–219.

19 Chekir C, Nakatsuka M, Noguchi S, Konishi H, Kamada Y, Sasaki A, Hao L, Hiramatsu Y: Accumulation of advanced glycation end products in women with preeclampsia: possible involvement of placental oxidative and nitrative stress. *Placenta* 2006; 27:225–233.

20 Cooke CL, Brockelsby JC, Baker PN, Davidge ST: The receptor for advanced glycation end products (RAGE) is elevated in women with preeclampsia. *Hypertens Pregnancy* 2003; 22:173–184.

21 Wang X, Athayde N, Trudinger B: Placental vascular disease and toll-like receptor 4 gene expression. *Am J Obstet Gynecol* 2005; 192:961–966.

22 Kim YM, Romero R, Oh SY, Kim CJ, Kilburn BA, Armant DR, Nien JK, Gomez R, Mazor M, Saito S, Abrahams VM, Mor G: Toll-like receptor 4: a potential link between "danger signals," the innate immune system, and preeclampsia? *Am J Obstet Gynecol* 2005; 193:921–927.

23 Holmlund U, Wahamaa H, Bachmayer N, Bremme K, Sverremark-Ekstrom E, Palmblad K: The novel inflammatory cytokine high mobility group box protein 1 (HMGB1) is expressed by human term placenta. *Immunology* 2007; 122:430–437.

24 Zicari A, Centonze C, Realacci M, Buchetti B, Pietropolli A, Ticconi C: Estradiol 17-beta and progesterone modulate inducible nitric oxide synthase and high mobility group box 1 expression in human endometrium. *Reprod Sci* 2008; 15:559–566.

25 Scaffidi P, Misteli T, Bianchi ME: Release of chromatin protein HMGB1 by necrotic cells triggers inflammation. *Nature* 2002; 418:191–195.

26 Gauley J, Pisetsky DS: The translocation of HMGB1 during cell activation and cell death. *Autoimmunity* 2009; 42:299–301.

27 Tsung A, Klune JR, Zhang X, Jeyabalan G, Cao Z, Peng X, Stolz DB, Geller DA, Rosengart MR, Billiar TR: HMGB1 release induced by liver ischemia involves Toll-like receptor 4 dependent reactive oxygen species production and calcium-mediated signaling. *J Exp Med* 2007; 204:2913–2923.

28 Germanova A, Koucky M, Hajek Z, Parizek A, Zima T, Kalousova M: Soluble receptor for advanced glycation end products in physiological and pathological pregnancy. *Clin Biochem* 2010; 43:442–446.

29 Pijnenborg R, McLaughlin PJ, Vercruysse L, Hanssens M, Johnson PM, Keith JC Jr, Van Assche FA: Immunolocalization of tumour necrosis factor-alpha (TNF-alpha) in the placental bed of normotensive and hypertensive human pregnancies. *Placenta* 1998; 19:231–239.

30 Lockwood CJ, Yen CF, Basar M, Kayisli UA, Martel M, Buhimschi I, Buhimschi C, Huang SJ, Krikun G, Schatz F: Preeclampsia-related inflammatory cytokines regulate interleukin-6 expression in human decidual cells. *Am J Pathol* 2008; 172:1571–1579.

31 Fiore G, Florio P, Micheli L, Nencini C, Rossi M, Cerretani D, Ambrosini G, Giorgi G, Petraglia F: Endothelin-1 triggers placental oxidative stress pathways: putative role in preeclampsia. *J Clin Endocrinol Metab* 2005; 90:4205–4210.

32 Whitley GS, Dash PR, Ayling LJ, Prefumo F, Thilaganathan B, Cartwright JE: Increased apoptosis in first trimester extravillous trophoblasts from pregnancies at higher risk of developing preeclampsia. *Am J Pathol* 2007; 170:1903–1909.

33 Crocker IP, Cooper S, Ong SC, Baker PN: Differences in apoptotic susceptibility of cytotrophoblasts and syncytiotrophoblasts in normal pregnancy to those complicated with preeclampsia and intrauterine growth restriction. *Am J Pathol* 2003; 162:637–643.

34 Mor G: Inflammation and pregnancy: the role of toll-like receptors in trophoblast-immune interaction. *Ann N Y Acad Sci* 2008; 1127:121–128.

35 Johansen M, Redman CW, Wilkins T, Sargent IL: Trophoblast deportation in human pregnancy – its relevance for pre-eclampsia. *Placenta* 1999; 20:531–539.

36 Voll RE, Urbonaviciute V, Herrmann M, Kalden JR: High mobility group box 1 in the pathogenesis of inflammatory and autoimmune diseases. *Isr Med Assoc J* 2008; 10:26–28.

37 Fukami A, Adachi H, Yamagishi S, Matsui T, Ueda S, Nakamura K, Enomoto M, Otsuka M, Kumagae S, Nanjo Y, Kumagai E, Esaki E, Murayama K, Hirai Y, Imaizumi T: Factors associated with serum high mobility group box 1 (HMGB1) levels in a general population. *Metabolism* 2009; 58:1688–1693.

Recruitment of CCR6-Expressing Th17 Cells by CCL 20 Secreted from IL-1β-, TNF-α-, and IL-17A-Stimulated Endometriotic Stromal Cells

Tetsuya Hirata, Yutaka Osuga, Masashi Takamura, Ako Kodama, Yasushi Hirota, Kaori Koga, Osamu Yoshino, Miyuki Harada, Yuri Takemura, Tetsu Yano, and Yuji Taketani

Department of Obstetrics and Gynecology, Faculty of Medicine, University of Tokyo, Tokyo 113-8655, Japan

In a novel paradigm of T cell differentiation, type 17 T helper (Th17) cells may play a significant role in endometriosis, a chronic inflammatory disease. However, the mechanism regulating the accumulation of Th17 cells in endometriotic tissues remains unknown. We hypothesized that Th17 cells migrate to endometriotic tissues through an interaction of the chemokine CC chemokine ligand (CCL)20 and its receptor CCR6. Using endometriotic tissues from women with endometriosis, we demonstrated, by flow cytometry, that Th17 cells in endometriotic tissues express CC chemokine receptor (CCR)6. Immunohistochemistry also revealed that CCL20 was expressed in the epithelial cells and stromal cells beneath the epithelium of endometriotic tissues. CCR6+ cells were small and round and scattered in the stroma in which abundant CCL20+ cells were detected. CCL20 caused selective migration of Th17 cells in the peripheral blood in a migration assay. IL-1β, TNF-α, and IL-17A increased the secretion of CCL20 in cultured endometriotic stromal cells. Inhibitors of p38- and p42/44-MAPKs, and stress-activated protein kinase/c-Jun kinase suppressed the secretion of CCL20 increased by IL-1β, TNF-α, and IL-17A. This suggests that the CCL20/CCR6 system is involved in the migration of Th17 cells to endometriotic tissues and that proinflammatory cytokines contribute to the development of endometriosis via up-regulation of CCL20 secretion from endometriotic stromal cells. (***Endocrinology*** **151: 5468–5476, 2010)**

Endometriosis is an enigmatic disease that deteriorates the health of women during their reproductive years by causing pain, infertility, and adnexal mass. Although the etiology of the disease still remains to be elucidated, a large volume of evidence indicates that inflammatory mediators and immune responses play crucial roles in the development of endometriosis (1, 2). In particular, various immune cells present in endometriotic tissues and their cytokines have been noted to play a significant role in the pathogenesis of endometriosis (3). Whereas the macrophage has been reported to be a typical immune cell involved in endometriosis, accumulating evidence in recent years extends the types of endometriosis-associated immune cells (4). Type 17 T helper (Th17) cells, regulatory T cells, and dendritic cells are new members of the group of immune cells suggested to contribute to the pathophysiology of the disease (5–7). We have already reported that Th2 cells and Th17 cells are potent inducers of inflammation associated with endometriosis (5, 8, 9).

Th17 cells are a novel subset of T lymphocytes that were thought to be composed of only Th1 and Th2 cells (10). A pivotal contribution of Th17 cells has been demonstrated in many chronic inflammatory diseases, such as rheumatoid arthritis, psoriasis, Crohn's disease, and multiple sclerosis as well as in host defenses against certain pathogens (11–14). Th17 cells exert multiple functions via their specific cytokine, IL-17A, which provokes a wide range of inflammatory reactions. We have detected Th17

ISSN Print 0013-7227 ISSN Online 1945-7170
Printed in U.S.A.

doi: 10.1210/en.2010-0398 Received April 8, 2010. Accepted August 24, 2010.
First Published Online September 29, 2010

Abbreviations: CCL, CC chemokine ligand; CCR, CC chemokine receptor; DMEM/F12, DMEM/Ham's F12 medium; EMMC, mononuclear cells from endometriotic lesions; ESC, endometriotic stromal cell; FBS, fetal bovine serum; JNK, c-Jun kinase; PBMC, peripheral blood mononuclear cell; PMA, phorbol 12-myristate 13-acetate; SAPK, stress-activated protein kinase; Th17, type 17 T helper.

cells in endometriosis-associated peritoneal fluid and endometriotic tissues and demonstrated the significant role of IL-17A in endometriosis by showing that IL-17A stimulates IL-8 and cyclooxygenase-2 expression and cell proliferation of endometriotic stromal cells (ESCs) (5).

Despite the important role of Th17 cells in endometriotic tissues, the mechanism by which these cells appear in the endometriotic tissues is unknown. A recent study in a mouse model of rheumatoid arthritis has shown that Th17 cells express CC chemokine receptor (CCR)6 and synoviocytes express CC chemokine ligand (CCL)20, the only chemotactic ligand for CCR6, suggesting CCL20-induced recruitment of Th17 cells to the inflamed joints (15). This study led us to hypothesize that endometriotic cells may express CCL20, causing CCR6-expressing Th17 cells to be recruited to the lesion. To address this issue, we examined the expression of CCR6 in Th17 cells and CCL20 in stromal cells in endometriotic tissues. We then studied the regulatory mechanism of secretion of CCL20 from cultured ESCs to address the involvement of the CCL20/CCR6 system in the pathophysiology of endometriosis.

Materials and Methods

Patients and samples

Endometriotic tissues and peripheral blood were obtained from patients with ovarian endometriomas undergoing laparoscopy. The severity of the disease was determined according to the revised classification of the American Society for Reproductive Medicine. The diagnosis of endometriosis was confirmed by histopathological examination. Laparoscopic excision of ovarian endometriomas was performed as follows. After inspection of the pelvis, the ovary was freed from any adhesions. The endometrioma cyst wall was stripped away from the normal ovarian tissue gently and completely. Endometriotic tissue samples were obtained from the excised cyst wall of the ovarian endometrioma and transported to the laboratory in DMEM/Ham's F12 medium (DMEM/F12; Invitrogen, Rockville, MD) on ice under sterile conditions. Peripheral blood was obtained from patients who were diagnosed as stage III or IV. All patients had regular menstrual cycles, and none had received hormonal treatment for at least 6 months before surgery. Peripheral blood was collected under sterile conditions before any manipulative procedure. Peripheral blood mononuclear cells (PBMCs) were isolated by standard Ficoll-Paque density centrifugation. The experimental procedures were approved by the Institutional Review Board of the University of Tokyo (Tokyo, Japan), and signed informed consent for use of the endometriotic tissues and blood samples was obtained from each patient.

Isolation of mononuclear cells from endometriotic lesions

Fresh endometriotic tissues collected in sterile medium were rinsed to remove red blood cells. The tissues were minced into small pieces and incubated in phenol red-free DMEM/F12 containing 0.25% type I collagenase (Wako Pure Chemical Industries, Osaka, Japan) and deoxyribonuclease I (15 IU/ml; Invitrogen) for 120 min at 37 C. The resulting dispersed cells were separated by filtration through 100- and 70-μm nylon cell strainers (Becton Dickinson and Co., Franklin Lakes, NJ). The filtrate was washed twice with PBS. This pellet was resuspended in 40% Percoll (5 ml), layered gently onto 70% Percoll, and centrifuged at 1800 rpm for 20 min. The interface was recovered and washed in PBS, resuspended in RPMI 1640 medium containing 10% charcoal-stripped fetal bovine serum (FBS; Hyclone, Logan, UT), and plated into 100-mm plates (Iwaki; Asahi Technology Co., Tokyo, Japan) and allowed to adhere at 37 C overnight. Nonadherent cells were collected and used for the experimental procedures as mononuclear cells from endometriotic lesions (EMMCs).

Immunohistochemistry

Paraffin-embedded specimens were sliced at 5-μm thickness and the sections placed on slides that were then deparafinized and rehydrated. Antigens were retrieved by buffer at 98 C. Endogenous peroxidase was blocked by incubation for 10 min with a solution of 0.3% hydrogen peroxidase. Immunohistochemical tissue labeling for CCL20 was performed using the avidin-biotin peroxidase method. After blocking with normal rabbit serum (Vector Laboratories, Burlingame, CA), the sections were incubated with 2 μg/ml goat antihuman CCL20 antibody (R & D Systems, Minneapolis, MN) or goat IgG (R & D Systems) for 60 min at room temperature and incubated with the avidin-biotin peroxidase complex (Vectastain Elite; Vector Laboratories), according to the manufacturer's instructions. The pattern of immunoreactivity was visualized using Vector VIP (Vector Laboratories) as substrate. Immunohistochemical tissue labeling for CCR6 was performed using EnVision+ (Dako, Glostrup, Denmark). After blocking with a nonspecific staining blocking reagent (Dako), the sections were incubated with 2 μg/ml rabbit antihuman CCR6 antibody (GeneTex, Irvine, CA) or rabbit IgG (Dako) for 60 min at room temperature and then incubated with peroxidase-conjugated secondary antibody for 30 min. Staining was detected using diaminobenzidine chromogen for a few minutes. All sections were counterstained with hematoxylin and evaluated under a light microscope.

Flow cytometric analysis

PBMCs or EMMCs were resuspended in 10% FBS in RPMI 1640 medium. The cells were stimulated with 50 ng/ml of phorbol 12-myristate 13-acetate (PMA; Sigma, St. Louis, MO) and 1 μg/ml of ionomycin (Sigma) for 5 h in the presence of Goldistop (BD Biosciences, San Jose, CA). Cells were first stained extracellularly with anti-CD3, anti-CD4, or anti-CCR6 antibodies (BD Biosciences) and then fixed and permeabilized with Perm/Fix solution (eBioscience, San Diego, CA) and finally stained intracellularly with antihuman IL-17A antibody (eBioscience). Samples were analyzed using FACSCalibur (BD Biosciences) and Cell Quest Pro (BD Biosciences).

Migration assay

Migration assays were performed on PBMCs using the Transwell system (5 μm pore size; Corning, Acton, MA). PBMCs (1×10^6) in 100 μl of RPMI 1640 medium containing 0.5% BSA (RPMI 1640–0.5% BSA) were placed in each Transwell insert. The Transwell inserts were placed in 24-well plates containing 600 μl of RPMI 1640–0.5% BSA with or without CCL20. After

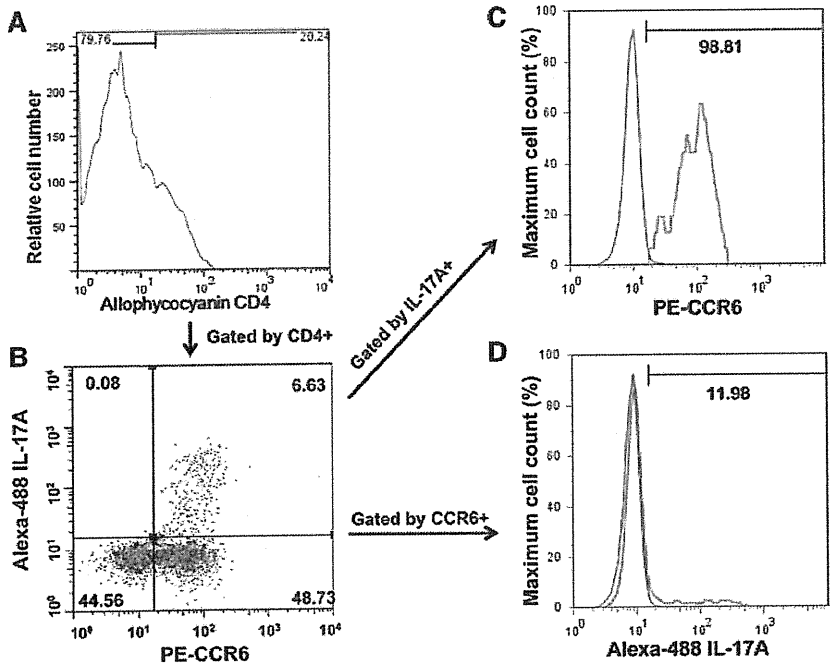

FIG. 1. Expression of CCR6 in Th17 cells in endometriotic tissues. Mononuclear cells from endometriotic lesions were stimulated with PMA (50 ng/ml) and ionomycin (1 μg/ml) and labeled with antibodies specific to lymphocytes (CD3 and CD4), IL-17A, and CCR6. A, The frequency of CD4+/CD3+ T cells from the lymphoid gates was determined by forward scatter and side scatter and by CD3+. B, Th17 cells were positive for CD3, CD4, and IL-17A; 6.63% of CD3+/CD4+ T cells were CCR6+/IL-17A+ cells. C, Of the Th17 cells, 98.81% were CCR6+ cells (*green line*). The *red line* represents the isotype-matched control. D, Th17 cells are 11.98% of CD3+, CD4+, and CCR6+ cells (*green line*). The *red line* represents the isotype-matched control. The data shown are representative of four separate experiments using samples from four different women.

incubation at 37 C in 5% CO_2 for 2 h, cells in the lower wells were collected. These cells were stimulated with PMA (50 ng/ml) and ionomycin (1 μg/ml) for 5 h in the presence of Goldistop and then stained with anti-CD3, anti-CD4, and anti-IL-17A, as described above. The absolute number of cells was counted and calculated using the Perfect Count System (Cytognos, Salamanca, Spain) (16). To calculate the migration index, the number of migrated cells for CCL20 was divided by the number of migrated cells for the control medium.

Isolation and culture of ESCs

Isolation and culture of human ESCs were performed as described previously (5, 17, 18). Briefly, fresh endometriotic tissues collected in sterile medium were rinsed to remove blood cells and then minced into small pieces and incubated in phenol red-free DMEM/F12 containing type I collagenase (0.25%) and deoxyribonuclease I (15 IU/ml) for 120 min at 37 C. The resulting dispersed endometriotic cells were separated by filtration through 100- and 70-μm nylon cell strainers. Stromal cells remaining in the filtrate were collected by centrifugation, resuspended in phenol red-free DMEM/F12, and plated into 100-mm dishes (Iwaki; Asahi Technology) and allowed to adhere at 37 C for 12 h. At the first passage, the cells were plated into 48-well plates at 1×10^5 cells/well. The cells reached confluence in 2–3 d and were then used for the experiments. The purity of ESCs was more than 95%, as judged by positive cellular staining for vimentin and negative cellular staining for cytokeratin, CD45, CD68, and von Willebrand factor.

Treatment of cultured ESCs

First, to examine the effect of IL-1β, TNF-α, or IL-17A on CCL20 production, the ESCs were incubated for 24 h in 5% FBS in DMEM/F12 with varying doses of IL-1β, TNF-α, or IL-17A (R & D Systems). Second, to examine the effects of MAPK inhibitors, three MAPK inhibitors (SB202190, PD98059, and SP600125; Calbiochem, La Jolla, CA) were added 1 h before the addition of IL-1β, TNF-α, or IL-17A, and the cells were incubated for 24 h. Finally, to evaluate the synergistic effect of TNF-α and IL-17A on CCL20 production, the cells were stimulated with varying doses of IL-17A (1–100 ng/ml) with or without TNF-α (1 ng/ml).

Measurement of CCL20

The concentration of CCL20 in conditioned media was measured using a specific ELISA kit (R & D Systems). The sensitivity of the assay was 0.5 pg/ml. The intraassay and interassay coefficients of variation were less than 5%.

Statistical analysis

Data were evaluated using ANOVA with Scheffé's *post hoc* analysis for multiple comparisons and *t* tests for two groups. $P < 0.05$ was accepted as statistically significant.

Results

Expression of CCR6 on Th17 cells in endometriotic tissues

Representative data showed that 20.24% of the CD3+ mononuclear cells in the EMMC samples were also CD4+ (Fig. 1A). Of these CD3+/CD4+ cells, 6.63% were IL-17A+/CCR6+ cells (Fig. 1B). Sequential gating revealed that expression of CCR6 was detected in 98.8% of Th17 cells (CD3+/CD4+/IL-17A+ cells, Fig. 1C) and that 11.98% of CD3+/CD4+/CCR6+ EMMCs were Th17 cells (Fig. 1D). The percentages of each figure were 38.1 ± 15.6, 7.85 ± 2.04, 97.6 ± 3.1, and 14.7 ± 5.1 (mean ± SD) for Fig. 1, A–D, respectively, from four independent experiments using samples from different women.

In vivo expression of CCL20 and CCR6 in endometriotic lesions

As shown in Fig. 2A, the presence of CCL20 immunoreactivity was detected in the cyst wall of endometriomas. Intense CCL20 immunoreactivity was detected in the epithelial cells and the stromal cells immediately beneath the epithelium. A few CCL20-immunoreactive cells were detected in fibrotic stromal cells, far from the

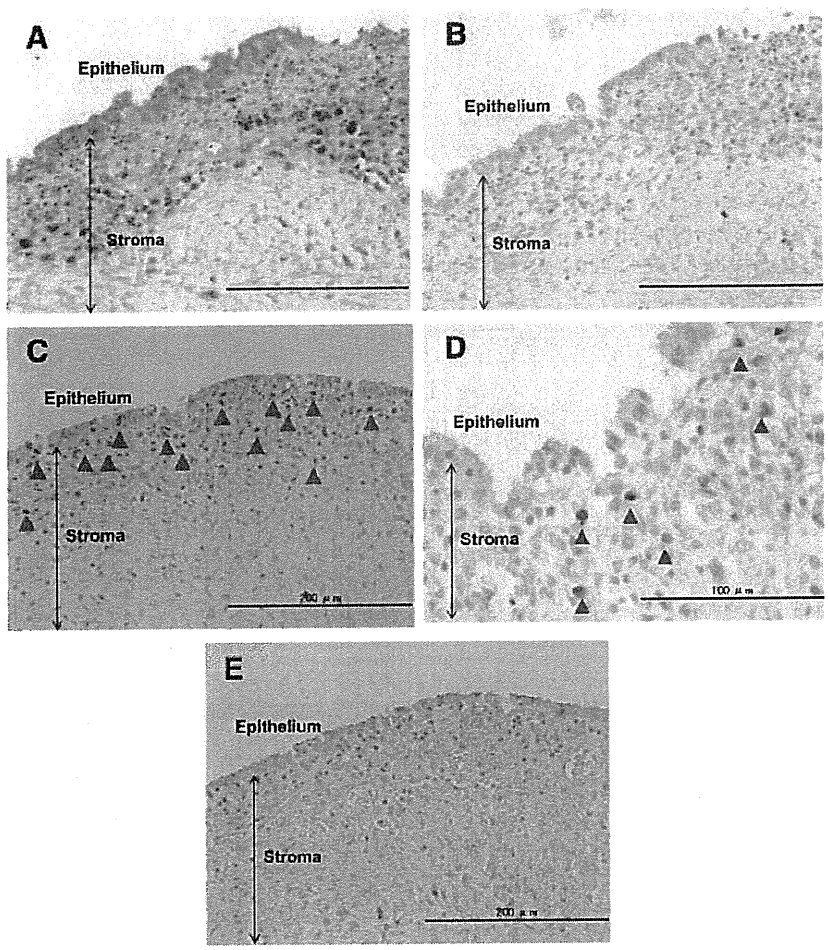

FIG. 2. Immunohistological localization of CCL20 and CCR6 in human endometriotic tissues. A and B, CCL20 expression (*purple*) was detected in human endometriotic tissues. Sections were immunostained with antihuman CCL20 antibody (A) or control goat IgG (B). Magnification, × 200; *scale bars*, 200 μm. C, D, and E, CCR6 expression (*brown*) was detected in human endometriotic cells. Sections were immunostained with antihuman CCR6 antibody (C and D) or control rabbit IgG (E). *Orange arrows* show CCR6+ cells. Magnification, × 200 (C and E), ×400 (D); *scale bars*, 200 μm (C and E), 100 μm (D).

epithelium. No staining was observed when normal goat IgG was used as a primary antibody, as shown in Fig. 2B. CCR6 immunoreactivity was also detected in the cyst wall of endometriomas (Fig. 2, C and D). CCR6+ cells were localized in the stroma immediately beneath the epithelium. These cells were round in shape and appeared to be bone marrow-derived cells. No staining was observed when normal rabbit IgG was used as a primary antibody, as shown in Fig. 2E.

Preferential migration of Th17 cells to CCL20

The function of CCR6 on T cells from PBMC samples was tested by migration assays using the Transwell system. Migrated cells were stimulated by PMA and ionomycin, and stained with CD3, CD4, and IL-17A antibodies. As shown in Fig. 3A, Th17 cells were more plentiful among the cells migrating to CCL20 (1000 ng/ml) than to the control medium. The absolute number of Th17 cells and CD4+ T cells was counted using Perfect Count (Cytognos). In Fig. 3B the data are presented as migration indexes. CCL20 (1000 ng/ml) significantly increased the migration index of the Th17 cells to 18.2-fold of control. In contrast, CCL20 at the same dose appeared to slightly increase the migration index of CD4+ cells, although without reaching statistical significance, indicating that CCL20 selectively enhances the migration of Th17 cells.

Effect of IL-1β, TNF-α, and IL-17A on CCL20 secretion by ESCs

The cytokines IL-1β, TNF-α, and IL-17A all enhanced CCL20 secretion from ESCs in a dose-dependent manner. IL-1β, at doses of 1 ng/ml and higher, significantly enhanced the secretion of CCL20 from ESCs (Fig. 4A). TNF-α (0.1 ng/ml and higher) and IL-17A (1 ng/ml and higher) also significantly enhanced the secretion of CCL20 from ESCs (Fig. 4, B and C).

Effect of MAPK inhibitors on IL-1β-, TNF-α-, and IL-17A-induced CCL20 secretion

We have previously demonstrated that IL-1β, TNF-α, and IL-17A activate p42/44-MAPK, p38-MAPK, and stress-activated protein kinase (SAPK)/c-Jun kinase (JNK). Thus, we examined in this study whether activation of these MAPKs was functionally linked to IL-1β-, TNF-α-, or IL-17A-induced production of CCL20. ESCs were treated with specific inhibitors of these pathways before stimulation with IL-1β, TNF-α, or IL-17A. As shown in Fig. 5, A–C, the addition of inhibitors for p38-MAPK, p42/44-MAPK, or SAPK/JNK significantly diminished the IL-1β-, TNF-α-, and IL-17A-induced increases in CCL20 secretion.

Synergistic effect of IL-17A and TNF-α on CCL20 secretion from ESCs

We examined the effect of TNF-α, a representative proinflammatory cytokine in endometriosis, on IL-17A-induced CCL20 secretion. TNF-α, together with IL-17A, triggered CCL20 secretion greater than the combined levels generated by each stimulus alone (Fig. 6). This synergistic effect was apparent when TNF-α was combined

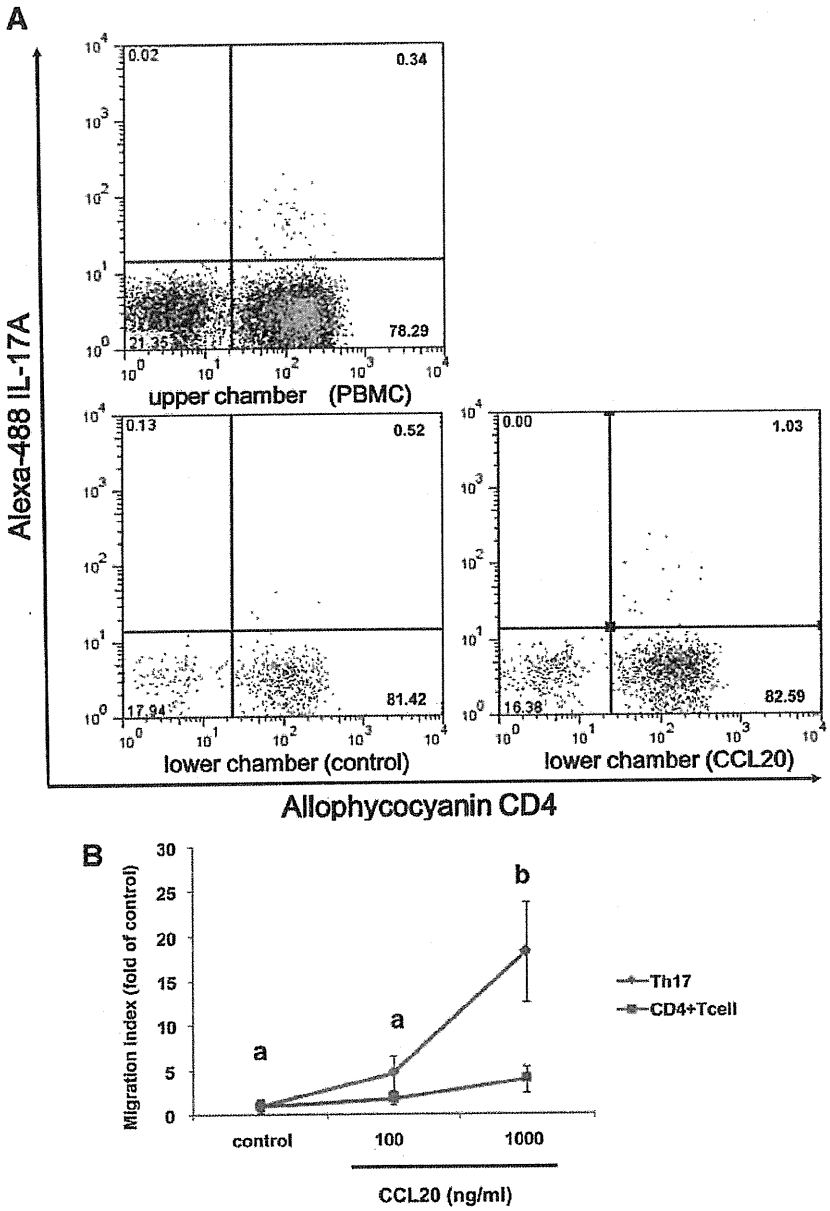

FIG. 3. Migration of Th17 cells in PBMCs to CCL20. A, Flow cytometry analysis of PBMCs from endometriotic women. PBMCs were applied to the upper chamber, and the cells migrated to the lower chamber with control medium (RPMI 1640–0.5% BSA) or medium containing CCL20 (1000 ng/ml). The cells were stimulated with PMA (50 ng/ml) and ionomycin (1 μg/ml) and stained with CD3, CD4, and IL-17A antibodies before flow cytometry. The percentage of cells in each quadrant was noted. B, Migration of Th17 cells or CD4+ cells to CCL20. Migrated cells were counted using Perfect Count (Cytognos). The data are presented as the migration index (ratio of cells migrating to CCL20 divided by cells migrating to the control medium). Values are expressed as the mean ± SEM of five independent experiments using samples from five different women. For CD4+ cells, there is no significant difference between the groups. *Different letters* denote significant differences between the groups ($P < 0.05$).

with 1 ng/ml IL-17A, and maximal synergy was obtained at the highest dose of IL-17A tested (100 ng/ml). Furthermore, we examined whether the MAPK inhibitors diminished TNF-α- and IL-17A-induced CCL20 secretion. CCL20 secretion induced by a combination of TNF-α and IL-17A was significantly suppressed by inhibitors for p38-MAPK, p42/44-MAPK, and SAPK/JNK (Fig. 6B).

Discussion

In the present study, we have demonstrated that Th17 cells express CCR6 in endometriotic tissues. Expression of CCL20, a ligand for CCR6, was also detected in the endometriotic stromal cells and epithelial cells, and CCL20 induced chemotaxis of Th17 cells from peripheral blood. IL-1β, TNF-α, and IL-17A increased secretion of CCL20 from cultured ESCs, and these effects were diminished by three MAPK inhibitors. Furthermore, TNF-α and IL-17A synergistically induced secretion of CCL20 from ESCs.

This study provides a possible explanation for why Th17 cells are present in endometriotic tissues. First, almost all of the Th17 cells in the endometriotic lesions expressed CCR6, consistent with reports describing this chemokine receptor as a marker for the identification of Th17 cells (19–22). Second, CCL20 and CCR6 expression was detected in the same part of the endometriotic lesion. Accordingly, we suggest that CCL20 expressed in endometriotic tissues recruits Th17 cells expressing CCR6. Indeed, CCL20 stimulated migration of Th17 cells in the peripheral blood of women with endometriosis. This notion is also supported by the localization of IL-17A+ cells. Our previous data showed that IL-17A+ cells were present mainly in the stroma just beneath the epithelium. The present study demonstrates that CCR6+ cells are also abundant in the stroma close to the epithelium. Because intense CCL20 immunostaining was observed in the epithelia and its nearby stroma, it is plausible that a CCL20/CCR6 interaction recruits Th17 cells to endometriotic tissues.

Today it is well established that endometriosis is an inflammatory disease. A large body of evidence indicates that TNF-α and IL-1β, typical inflammatory cytokines,

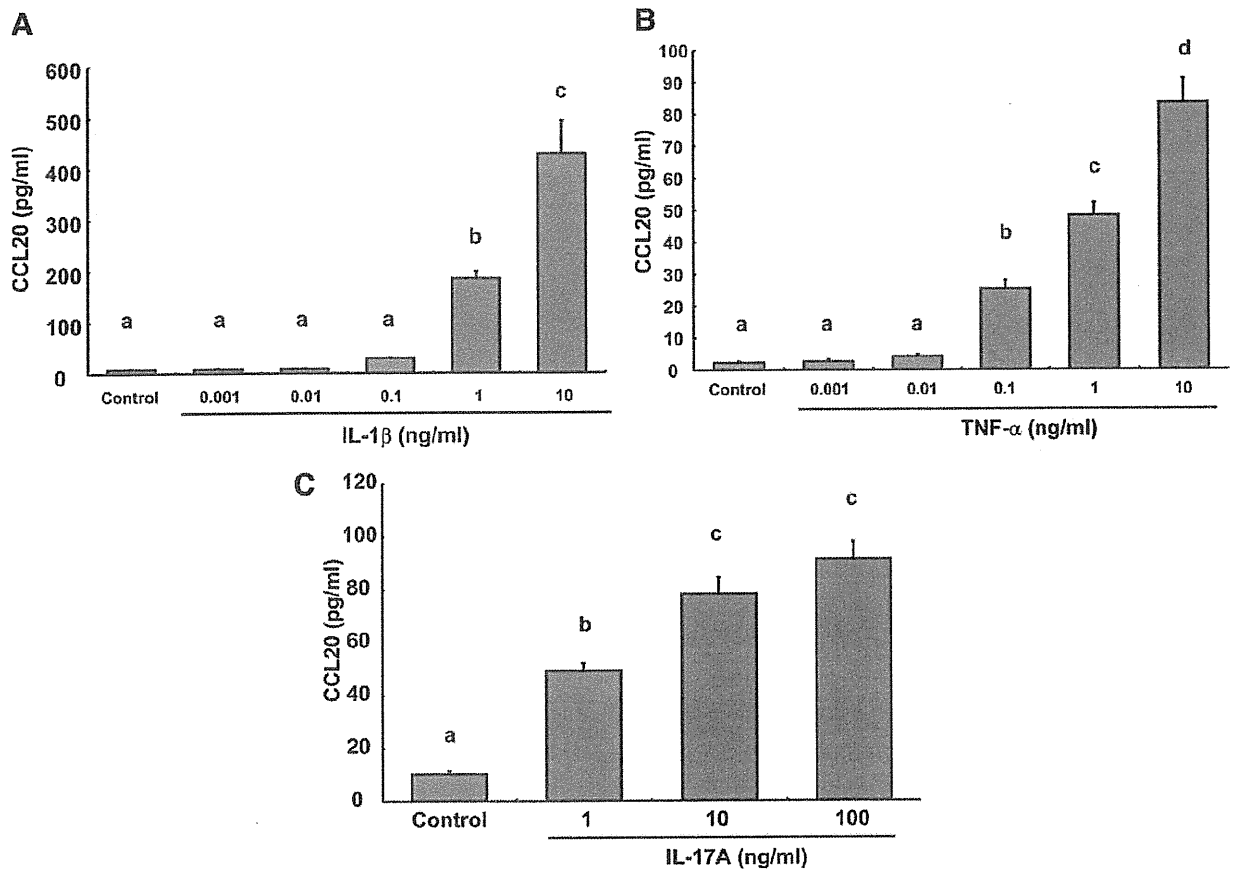

FIG. 4. The effect of IL-1β (A), TNF-α (B), and IL-17A (C) on secretion of CCL20 in ESCs. ESCs were cultured in 5% FBS with different doses of IL-1β, TNF-α, or IL-17A for 24 h. The concentration of CCL20 in the conditioned medium was measured using a specific ELISA. Values are expressed as the mean ± SEM of five identical cultures. These results are representative of five (A) or four (B and C) separate experiments using samples from different patients. *Different letters* denote significant differences between the groups ($P < 0.05$).

are involved in macrophage activation, inflammatory change, and enhanced angiogenesis to develop endometriosis (3). A pivotal role of TNF-α in endometriosis is corroborated by the finding that TNF-α-targeted suppression by specific drugs inhibits the development of endometriosis in baboons (23, 24). In addition to TNF-α and IL-1β, we have recently shown that IL-17A is also involved in the pathogenesis of endometriosis, stimulating IL-8 secretion, cyclooxygenase-2 expression, and cell proliferation of ESCs (5). The present study revealed a novel function of these inflammatory cytokines: enhancement of CCL20 secretion from endometriotic stromal cells. Collectively, these results suggest that CCL20 expression in endometriotic tissues is regulated by these cytokines and that local inflammation may up-regulate CCL20 expression through these cytokines. In this context, Th17 cells themselves may sustain a positive feedback loop by secreting IL-17A, which further induces the accumulation of Th17 cells via an increase in CCL20 in endometriotic lesions.

Inspired by the finding that IL-1β, TNF-α, and IL-17A increased secretion of CCL20 from ESCs, we examined whether these cytokines stimulated CCR6 expression on Th17 cells using flow cytometry. However, these cytokines did not affect the CCR6 expression level on Th17 cells in endometriotic tissues (data not shown).

The synergistic effect of IL-17A and TNF-α to increase CCL20 secretion from ESCs is interesting. TNF-α, a proposed key molecule in the progression of endometriosis, as mentioned above, is produced by a range of leukocytes including neutrophils, activated lymphocytes, and macrophages. Of these cells, the macrophage is a well-known resident of endometriotic tissues and is suggested to play a central role in the immunobiology of endometriosis (25). Given that TNF-α is secreted from macrophages, it is possible that Th17 cells secreting IL-17A may act synergistically with macrophages to enhance CCL20 secretion and lead to enforced recruitment of Th17 cells. Consequently, this synergistic effect may augment the various effects of IL-17A on ESCs through the enhanced recruitment of Th17 cells.

We have previously shown that IL-1β, TNF-α, and IL-17A induce the phosphorylation of p42/44-MAPK, p38-MAPK, and SAPK/JNK in ESCs (5, 26). Inhibitors of these